The Astrophysical Journal, 683:55–69, 2008 August 10

ON THE CONNECTION BETWEEN METAL ABSORBERS AND QUASAR NEBULAE

Doron Chelouche,[1,2] Brice Ménard,[1,3] David V. Bowen,[4] and Orly Gnat[5,6]

Received 2007 March 1; accepted 2008 January 25

ABSTRACT

We establish a simple model for the distribution of cool ($\sim 10^4$ K) gas around $L^\star$ galaxies using the properties of strong Mg II absorption line systems as observational constraints. Our analysis suggests that the halos of $L^\star$ galaxies are filled with cool gas clouds having sizes of order 1 kpc and densities of $\sim 10^{-2}$ cm^{-3}. We then investigate the physical conditions of a similar ensemble of clouds situated around a central quasar. We show that the flux from the quasar gives rise to (1) extended narrow line emission on $\sim$100 kpc scales and (2) an anisotropy in the properties of the absorbing gas arising from the geometry of the quasar radiation field. Provided that quasars reside in gaseous halos more massive than those of $L^\star$ galaxies, our predictions agree with the results from detections of both narrow emission line nebulae and $\sim$100 kpc Mg II–absorbing halos around quasars, suggesting a common origin for these phenomena. We discuss the implications of our results for understanding quasar absorption line systems, quasar environments at high redshifts, and the quasar unification scheme.

Subject headings: atomic processes — galaxies: halos — quasars: absorption lines — quasars: emission lines

Online material: color figures

1. INTRODUCTION

Observational data on quasar absorption lines indicate that galaxies with $L^\star$ luminosities are surrounded by cool ($\sim 10^4$ K) gas condensations with radii of up to $\sim 100\, h_{70}^{-1}$ kpc (Bergeron et al. 1987; Churchill et al. 2005; Zibetti et al. 2006).[7] Similar distributions have recently been found around quasars (Bowen et al. 2006, 2007). In addition, bright quasars have also been found surrounded by giant line-emitting nebulae observed in transitions such as Lyα (e.g., Wampler et al. 1975; Heckman et al. 1991a, 1991b; Christensen et al. 2006). In this paper we investigate whether the two phenomena could originate from the same type of gas clouds around galaxies, thereby connecting gas absorption and line emission in galaxy and quasar halos.

Quasar spectra have historically been an important source of information about the large-scale matter distribution in the early universe. Such information has been obtained by studying absorption lines induced by intervening material between us and the quasar. In the optical wavelength range, one of the easiest absorption line species to detect is the Mg II $\lambda\lambda$2796, 2803 doublet. It is the first resonance transition of an abundant element with a large oscillator strength to enter the optical range and has therefore been the most commonly used tracer of cool gas. Several studies have shown that Mg II arises in gas spanning more than 5 orders of magnitude in neutral hydrogen column density, in the range $N_{\rm H\,I} \simeq 10^{17}$–$10^{22}$ cm^{-2} (Bergeron & Stasinska 1986; Steidel & Sargent 1992; Churchill et al. 2000). Following the suggestion by Bahcall & Spitzer (1969) that quasar absorption lines might arise in galactic halos, a direct association between Mg II absorbers and galaxies has been reported, either from searching for the galaxy responsible for an individual Mg II system (Bergeron 1986; Cristiani 1987; Bergeron & Boisse 1991; Steidel et al. 1997; Churchill et al. 2005) or by using statistical measurements involving thousands of objects (Zibetti et al. 2005, 2006; Ménard et al. 2007).

While a connection between galaxies and Mg II absorbers has been established, the origin of the absorbing gas remains unclear. Whether an absorption-line system traces gas being accreted by, or outflowing from, a galaxy is still a matter of debate. Possible origins for absorption-line systems in galaxy halos include condensations of cool clouds from hot and dilute halo gas via thermal instability (e.g., Mo & Miralda-Escude 1996; Maller & Bullock 2004), cool gas that is bound to dark matter subhalos embedded within the main halo (e.g., Sternberg et al. 2002 and references therein), and starburst-driven winds from galaxies (e.g., Oppenheimer & Davé 2006; Prochter et al. 2006). Additional explanations include (warped) galaxy disks (Bowen et al. 1995; Prochaska & Wolfe 1998), as well as low surface brightness companion objects (York et al. 1986; Petitjean & Bergeron 1994).

Some galaxies contain active nuclei, and it is thought that all quasars are harbored in galaxies. The properties of quasar hosts are not well characterized, but bright quasars usually reside in massive, star-forming galaxies ranging in luminosity from $\sim 1L^\star$ to $\sim 30L^\star$ (Jahnke & Wisotzki 2003). Little is known about the environments of quasars, although the brightest objects may live in somewhat overdense environments (Serber et al. 2006). Like galaxies, the immediate environment of quasars can also be probed in absorption. Recently, we identified projected quasar-quasar pairs in the Sloan Digital Sky Survey (SDSS) and detected Mg II–absorbing gas around the foreground quasars out to separations of 100 h_{70}^{-1} kpc (Bowen et al. 2006). Using a much larger sample of quasar pairs, we have now found that the transverse gas distribution around quasars, as traced by Mg II absorption lines, has a covering factor of order unity out to $\sim 100\, h_{70}^{-1}$ kpc (Bowen et al. 2007).

Gas that is associated more directly with the quasar itself is also commonly observed (via resonance absorption lines such as C IV $\lambda\lambda$1548, 1550) in lines of sight toward quasars and can be identified by its proximity (within $\sim 10^3$ km s^{-1}) to the quasar

[1] School of Natural Sciences, Institute for Advanced Study, Princeton, NJ 08540; doron@ias.edu.
[2] Chandra Fellow.
[3] Canadian Institute for Theoretical Astrophysics, University of Toronto, Toronto, ON M5S 3H8, Canada.
[4] Department of Astrophysical Sciences, Princeton University, Princeton, NJ 08544.
[5] School of Physics and Astronomy and the Wise Observatory, Tel-Aviv University, Tel-Aviv, Israel.
[6] Theoretical Astrophysics, California Institute of Technology, MC 130-33, Pasadena, CA 91125.
[7] Throughout the paper we use $H_0 = 70\, h_{70}$ km s^{-1} Mpc^{-1}, $\Omega_M = 0.7$, and $\Omega_\Lambda = 0.3$.

redshift. Nevertheless, it is generally hard to establish whether the gas in these "associated" absorption systems lies in the vicinity of the black hole (on subparsec scales) or whether it originates in its host galaxy or its surrounding halo (for a review see Crenshaw et al. 2003).

Deep imaging and spectroscopic observations of quasars reveal that a significant fraction of them have surrounding emission-line nebulosities extending out to $\sim 100\ h_{70}^{-1}$ kpc. Such nebulosities are often detected in Lyα emission (e.g., Heckman et al. 1991a, 1991b; Christensen et al. 2006) or the [O III] λ5007 line (Stockton & MacKenty 1987; Fu & Stockton 2006), with recent surveys suggesting that radio-loud quasars (RLQs) may have brighter Lyα nebulosities (Christensen et al. 2006). Little is known about the physical nature of these nebulae, and various scenarios pertaining to both gas accretion onto the quasar and gas ejection from it have been put forward as possible explanations (e.g., Heckman et al. 1991a, 1991b; Haiman & Rees 2001).

Motivated by these recent findings, we investigate in this work whether the emitting gas seen around quasars can arise from the same gas clouds as those detected in absorption around galaxies (and quasars). The paper is organized as follows: In § 2 we first summarize some observational constraints on the properties of cool gas around galaxies used to calibrate our model. A geometrical model is then constructed and its physics is discussed. We then (§ 3) use this model to study the effects on the absorption and emission properties of halo gas when exposed to a quasar radiation field. In addition, we show that such a model can naturally explain the distribution of cool gas around quasars and the existence of large-scale Lyα-emitting nebulae. We discuss the implications of our results for galaxy formation, baryon fraction in the universe, and quasar physics in § 4. A summary follows in § 5.

2. THE DISTRIBUTION OF COOL GAS AROUND $L^\star$ GALAXIES

2.1. *Observational Constraints from* Mg II *Absorbers*

Observational data on Mg II absorption lines have provided a number of constraints on the spatial distribution and characteristics of the cool gas around galaxies. Here we list the most relevant results that can be used to model the Mg II distribution in the halo of an $L^\star$ galaxy:

1. Strong Mg II systems (defined by the λ2796 line having a rest equivalent width $W_0 > 0.3$ Å) inhabit the halos of $\sim L^\star$ galaxies. Steidel et al. (1997) found that Mg II–selected galaxy luminosities lie in the range $0.3L^\star$–$5L^\star$ with a mean $\langle L \rangle \simeq 0.8L^\star$. Their results also suggested a unit covering factor up to $\sim 50\ h_{70}^{-1}$ kpc and the absence of strong Mg II absorption on larger scales. More recent studies by Zibetti et al. (2005, 2006) and Churchill et al. (2005) indicate that strong Mg II absorption can actually be detected at distances beyond $100\ h_{70}^{-1}$ kpc but that the covering factor falls off sharply in this range. Zibetti et al. (2006) found little evolution in the properties of absorbing galaxies out to redshifts $z \sim 1$.

2. High-resolution spectroscopy reveals that the strong Mg II systems usually break into several kinematically distinct, optically thick components (e.g., Churchill & Vogt 2001). When resolved, the Doppler widths of these components are consistent with gas at a temperature of $\sim 10^4$ K (e.g., Lanzetta & Bowen 1990). The total rest equivalent width of a strong Mg II line (a value independent of the spectral resolution at which it is observed) is roughly proportional to the number of kinematically distinct components that comprise the line. Petitjean & Bergeron (1990) found the relation between total rest equivalent width and number of clouds to be $W_0(\text{Mg II}) \simeq 0.3 N_c$ Å, and Churchill et al. (2003) reported $W_0(\text{Mg II}) \simeq 0.07 N_c$ Å, where N_c is the number of clouds along the line of sight. If the individual clouds observed in these systems are relatively similar, then these results suggest that, even if the rest equivalent width of Mg II systems is mostly driven by a velocity dispersion, it can be used as a proxy for the number of clouds along the line of sight.

3. Constraints on the sizes of Mg II absorbers have been obtained by studying the spectra of strongly lensed quasars. Limits on the size of individual absorbing clouds have been obtained by comparing absorption features across different lines of sight. Sizes of 0.1–10 kpc have been found for the Mg II–absorbing clouds (e.g., Rauch et al. 2002; Ellison et al. 2004), and perhaps somewhat larger sizes for systems detected by high-ionization lines such as C IV. At present this is the only direct means for estimating the size of cool gaseous clouds in galaxy halos (for an indirect method relying on photoionization modeling see, e.g., Ding et al. 2003).

4. Finally, H I measurements show that strong Mg II systems with $W_0 \sim 0.5$ Å arise in gas with H I column densities in the range 10^{18}–10^{20} cm^{-2}, while stronger systems with $W_0 \sim 2$ Å have $N_{\text{H I}} \sim 10^{19}$–$10^{21}$ cm^{-2} (Rao et al. 2006). Results from 21 cm surveys at $z = 0$ (Zwaan et al. 2005) indicate that the contribution of galaxy *disks* to the observed H I column density distribution can be substantial within $\sim$20 kpc for certain orientations (see also Bowen et al. 1995; Prochaska & Wolfe 1997). However, at larger radii, gas clouds in galactic halos are expected to dominate the H I column density distribution. The lack of correlation between Mg II absorption properties and galaxy size or inclination further supports this assertion (Steidel et al. 2002; see also Kacprzak et al. 2007).

2.2. *Modeling the Spatial Distribution*

We introduce a simple phenomenological model aimed at reproducing the main aspects of the observational constraints listed above: the spatial extent of the gas, the cross section for strong Mg II absorption, and the distribution of hydrogen column densities around $\sim L^\star$ galaxies inferred from the Mg II statistics. We emphasize that we do *not* attempt to constrain the physical origin of the gas, i.e., whether it is bound to satellite dark matter halos, is infalling, or is being ejected out of the galaxy via winds. We consider a case in which the total mass density (baryonic and dark matter) for such a system is described by an isothermal profile:

$$\rho(r) = \frac{\sigma^2}{2\pi G r^2}, \quad r \le r_v = \frac{\sigma}{\sqrt{50} H_0}, \tag{1}$$

where σ is the velocity dispersion, r_v is the virial radius, and ρ is the density. The mass within a given radius r is then given by

$$M(<r) = \frac{2\sigma^2 r}{G}, \tag{2}$$

and by definition, the density enclosed within the virial radius is 200 times the critical density. According to Fukugita & Peebles (2006), the velocity dispersion of late-type galaxy halos is $\simeq$140 km s^{-1}, which corresponds to a virial mass $M_\star \simeq 2.5 \times 10^{12}\ M_\odot$ within $r_v = 282$ kpc at $z = 0$ (there is little evolution in the physical properties of halos for $z < 1$; Diemand et al. 2007).

For simplicity we assume that the density of cool gas around $L^\star$ galaxies varies with radius as

$$\rho_{\text{cool}}(r) \propto r^{-2}. \tag{3}$$

Such a density profile arises naturally in a wide range of models for the origin of the absorbing gas. In particular, it characterizes

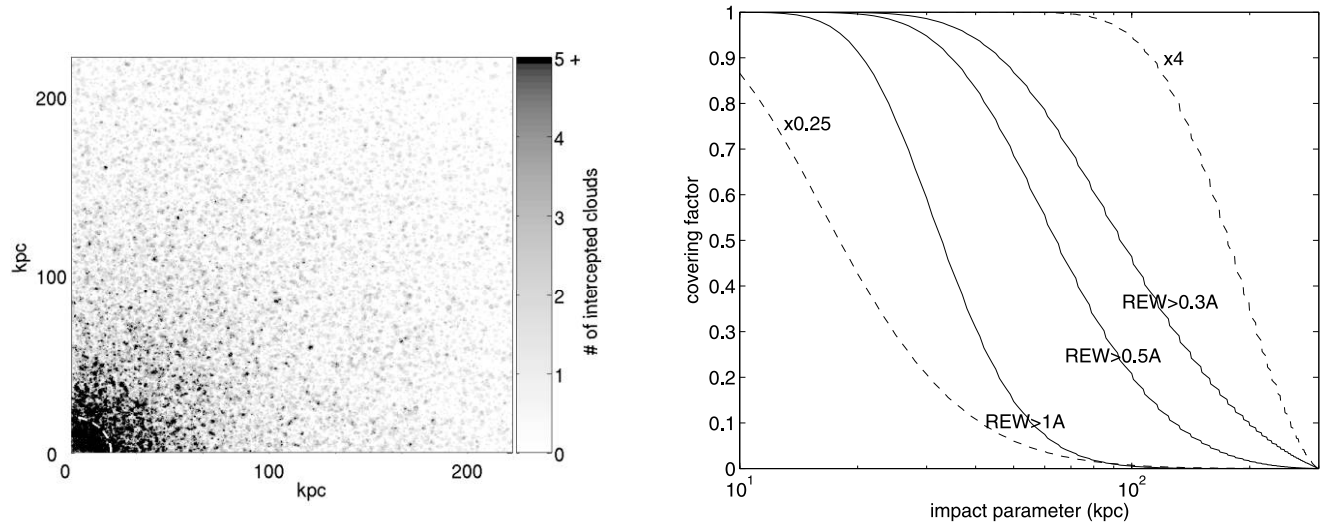

FIG. 1.—*Left*: Number count distribution of intercepted Mg II clouds along different lines of sight through a halo of an L^* galaxy (see text). As expected, the number of intercepted clouds increases with decreasing impact parameter. Clouds are also distributed out to the virial radius although the probability of intercepting one of them at these large radii is small. *Right*: Covering factor for strong Mg II absorption around galaxies. The different solid lines correspond to model predictions of the covering factor for different W_0 limits (denoted to the right of each curve) around an L^* galaxy. As shown, the covering factor for strong, $W_0 > 0.5$ Å absorption is below 50% for impact parameters greater than 50 kpc. Conversely, weak absorption with $W_0 < 0.3$ Å is common for impact parameters greater than 70 kpc. The dashed lines are model predictions for galaxy halo models with cool gas mass 0.25 and 4 times that of an L^* galaxy and for $W_0 > 0.5$ Å.

gas that follows the dark matter distribution in isothermal halos. It is also a property of mass-conserving outflowing winds or infalling gas (in spherical geometry) that holds over a range of radii where the velocity is roughly constant. As seen below, deviations from this power law do not significantly affect our conclusions.

The multiple components observed in high-resolution spectra indicate that the gas does not follow an overall smooth distribution but is distributed in discrete systems. To reproduce this property, we consider the cool gas to be in the form of clouds that are distributed within the halo following a Poisson distribution with a mean number density, $n_{\rm cloud}$, that follows $\rho_{\rm cool}(r)$. The number of clouds intercepted along a physical path dl along a line of sight through the gaseous halo of a galaxy is

$$dN_{\rm cloud} = n_{\rm cloud}(\boldsymbol{r})\pi R^2_{\rm cloud}\, d\boldsymbol{l}, \tag{4}$$

where πR^2 is the cloud cross section for inducing Mg II absorption, $\boldsymbol{r}$ is a vector from the halo center, and $d\boldsymbol{l}$ is measured along the line of sight. By integrating over the density profile of the gas, we find the number of clouds along a given line of sight at some impact parameter, b, to be

$$N_{\rm cloud}(b) = \frac{\pi}{2}\Psi\left(\frac{r_v}{b}\right) n_{\rm cloud}(b)\pi R^2 b, \tag{5}$$

where $\Psi(r_v/b) = (2/\pi)\int_1^{r_v/b} d\xi\, \xi^{-1}/(\xi^2-1)^{1/2}$.

As mentioned above, the overall rest equivalent width of strong Mg II systems is roughly proportional to the number of subcomponents. We can therefore use this empirical relation and approximate the rest equivalent width of the Mg II λ2796 line by

$$W_0 \simeq N_{\rm cloud} W_c, \tag{6}$$

with $W_c = 0.2$ Å. Here we have used the mean of the proportionality factors reported by Petitjean & Bergeron (1990) and Churchill et al. (2003).

The final constraint needed for our model is the normalization of the overall amplitude. Steidel (1993) has shown that Mg II absorption with $W_0 \gtrsim 0.5$ Å is found within $\sim$50 kpc of L^* galaxies with a unit covering factor. This imposes a constraint on our model: $\langle W_0(r = 50\ {\rm kpc})\rangle \simeq 0.5$ Å. Equation (6) implies that, on average, about two Mg II clouds are intercepted along any line of sight at an impact parameter of 50 kpc. More recent results by Zibetti et al. (2005) and Churchill et al. (2005) have shown that, in fact, absorption can be found out to impact parameters of more than 100 kpc, although the covering factor is less than unity at those distances. In our model, once the function $W_0(r)$ has been normalized at 50 kpc, the cloud distribution of Mg II systems automatically reproduces the drop in the covering factor for absorption and allows absorbing clouds to be found at impact parameters >100 kpc. The scatter in $W_0(b) \propto N_{\rm cloud}(b)$ is largely due to the relatively small number of clouds. Specifically, the standard deviation is given by $\{1 + [N_{\rm cloud}(b) + 0.75]^{1/2}\}W_c$ (Gehrels 1986) and is therefore considerable ($\Delta W_0/W_0 \lesssim 1$). Interestingly, a large scatter is also seen in the data, yet its magnitude is poorly constrained due to small number statistics per galaxy luminosity bin (Steidel 1993).

Given the properties of Mg II systems described above, the resulting cloud distribution is shown in Figure 1. The left panel shows the distribution of intercepted clouds of cool gas as a function of impact parameter, as well as the expected scatter. The right panel presents, for different absorption-line sensitivities, the covering factor for absorption around L^* galaxies. The observational constraints we are using are likely to be valid only at radii greater than $\sim$20 kpc, denoted in Figure 1 by a white dashed circle. At radii smaller than 20 kpc, the disks of late-type galaxies will contribute significantly to the Mg II absorption. In this paper we are only interested in the distribution of gas in the halo and will hence focus only on the absorption at these larger radii.

2.3. *Properties of* Mg II *Clouds*

We now investigate the possible range of physical conditions that allow the existence of Mg II clouds around a galaxy. Given the low gas temperatures associated with individual Mg II absorption components, we neglect effects from collisional heating by shocks, conduction, and cosmic-ray heating (e.g., Bergeron & Stasinska 1986; Charlton et al. 2000) and only consider the effects of photoionization. For clouds in a galactic halo, most of the ionizing flux originates from the metagalactic field (Haardt &

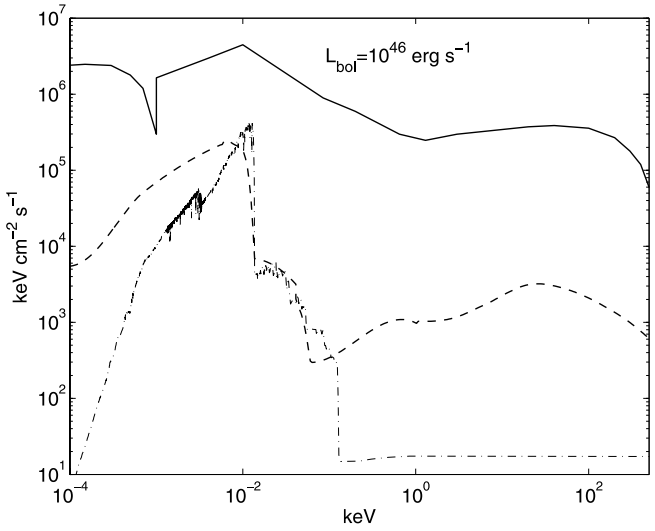

FIG. 2.—Various components of the ionizing radiation field considered in this work. The quasar SED (*solid line*), the galaxy ionizing radiation field (*dot-dashed line*), and the UV/X-ray background radiation field (*dashed line*) are shown. The relative normalizations of the different components were scaled to the values that would be measured at a distance of 50 kpc from the center of a galaxy (see text).

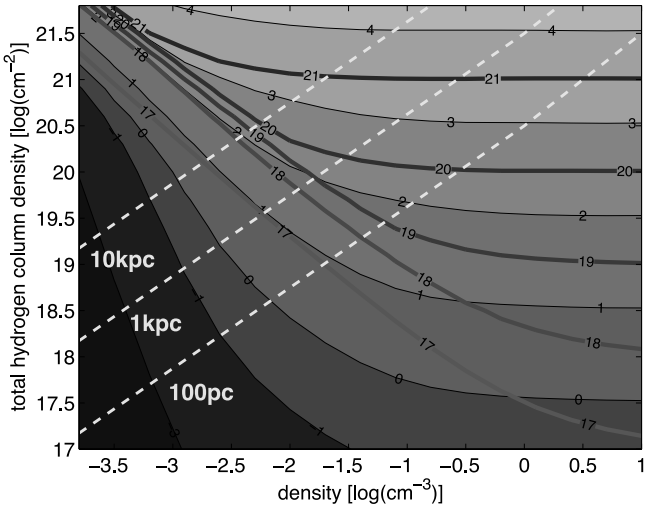

FIG. 3.—Contour plot of the Mg II λ2796 optical depth (*filled contours*) and the H I column density (*line contours*), both in logarithmic units, as a function of the cloud particle number density and total hydrogen column density. Only the UV/X-ray ionizing background radiation is assumed. Lines corresponding to several cloud sizes are also drawn (see text). [*See the electronic edition of the Journal for a color version of this figure.*]

Madau 1996) and the central galaxy. Contributions to the mean ionizing photon flux from satellite galaxies and other diffuse sources can be neglected. The background UV/X-ray ionizing radiation is due to quasars and stars. Characterizing this spectrum requires knowledge of the star formation rate and quasar activation history, as well as the opacity of intervening material. In this work we use the Haardt & Madau (1996, 2001) calculations and consider the background radiation at $z \sim 1$. The spectrum, integrated over 4π sr, is shown in Figure 2 with a dashed line.

In addition to diffuse background radiation, there is also the ionizing radiation from the central galaxy. We model the galaxy spectrum using the Bruzual & Charlot (1993) models and the Chabrier (2003) initial mass function. We assume gray opacity beyond the Lyman edge so that 5% of the ionizing continuum escapes to the halo (e.g., Bland-Hawthorn & Maloney 2001). A population of X-ray binaries is also included (Norman et al. 2004) using the infrared to X-ray scaling of Ranalli et al. (2003). The galaxy ionizing radiation is shown in Figure 2.

To model the photoionization and thermal equilibrium of the cool gas clouds in the halo, we use the Cloudy c06.02a photoionization code (Ferland et al. 1998) with the Badnell dielectronic recombination coefficients (Badnell 2006). We simplify the calculations by assuming a slab geometry with one surface of the cloud exposed to half of the total ionizing flux. Photoionization calculations are carried out to the center of the cloud, and symmetry is assumed when calculating the total column density of ions (for a more realistic treatment of the problem see Gnat & Sternberg 2004). We assume the gas to have 1/10 the solar metallicity (Turnshek et al. 2005; York et al. 2006).

We investigated several possible scenarios for the structure of the clouds, whereby they had (*a*) constant density; this is perhaps the simplest model yet has been the main route by which a wide range of astrophysical phenomena are modeled; (*b*) constant radiation and gas pressure; this may be relevant to clouds in pressure equilibrium with their surroundings (e.g., with the intercloud medium); and (*c*) constant temperature; this could be envisioned as gas that is collisionally heated to the virial temperature of dark matter minihalos. Given the parameter space of interest, our mean cloud is not very optically thick above the Lyman edge and so the different models do not give appreciably different results. For simplicity, we discuss only the results obtained for a constant density medium.

We have calculated the column density of Mg II and H I as a function of total (ionized plus neutral) hydrogen column density and the number density of particles. The results are shown in Figure 3.

We have repeated the calculations after including the effect of the ionizing radiation field of the galaxy and found it to be dominant within the central $\sim$40 kpc (see § 2.4 for the effect of cloud shielding). The gas considered here, having a low ionization level, is sensitive to the ionizing flux just above the Lyman edge. To first order, gas that is exposed to the galaxy ionizing flux (in addition to the UV background ionizing radiation flux, $f_{\rm UV}$), f_g, would attain a similar ionization structure to that shown in Figure 3 provided that its density is greater by a factor $1 + f_g/f_{\rm UV}$. Similarly, at higher redshifts, where the UV background radiation is stronger, the density of a cloud with a similar ionization level to that shown in Figure 3 would be higher by the UV flux ratio of the epochs.

Constraining the parameter range relevant to strong Mg II absorbers is not straightforward since strong Mg II lines are usually saturated and additional observational constraints are needed to estimate their typical density and column density. A useful constraint is the size of the clouds derived from strong-lensing studies. As noted above, such studies indicate that the size of Mg II absorbers is $\sim$1 kpc. This constraint substantially reduces the relevant parameter space in Figure 3. A second constraint comes from the H I column density measurements for strong Mg II absorbers (Rao et al. 2006; see Fig. 4). Using the rest equivalent width as a proxy for the column density along the line of sight (see eq. [6]), we see from Figure 4 that a typical cloud, giving rise to $W_0 = W_c \sim 0.2$ Å, has an H I column density of $\sim 10^{18}$ cm^{-2}, implying a density of about 2×10^{-2} cm^{-3}. Such values are consistent with previous estimates for the density of cool gas in galaxy halos (for the case of high-velocity clouds in the Galaxy see, e.g., Sternberg et al. 2002).

The scatter in the $N_{\rm H\,I}$ versus W_0 relation presented in Figure 4 is significantly larger than that of the simplified model presented in the previous section. Several effects not included in our model could contribute to this scatter: a distribution of galaxy masses, types, star formation histories, etc., all of which are beyond the

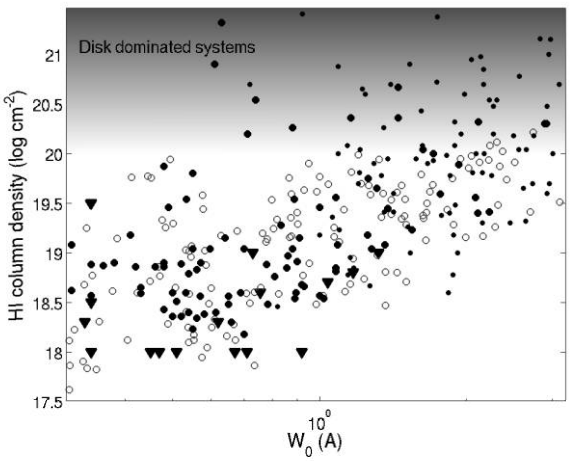

FIG. 4.—Plot of H I column density vs. the rest equivalent width of the Mg II λ2796 line for Mg II–selected systems (see Rao et al. 2006). Data appear as black points with upper limits marked by triangles. Different point sizes indicate different selection criteria employed by Rao et al. (2006) (large points are for systems selected by criteria 1 and 2, while smaller points are selected by criteria 3 and 4; see Rao et al. 2006); both sets of points have similar properties for the low column density range considered here. The contribution of galaxy disks to the measured H I column density may become important in the shaded region of the diagram (Zwaan et al. 2005); our model does not attempt to account for these column densities. The simulated data (*circles*) represent the summed H I column density of W_0/W_c clouds giving rise to W_0 Mg II absorption along the line of sight. The model reproduces the lower column density envelope (see text). [*See the electronic edition of the Journal for a color version of this figure.*]

scope of this paper. In the absence of a clear physical motivation, we attempt to take this effect into account by introducing a distribution of cloud sizes. Here clouds have similar densities and so have similar pressures, allowing them to be in pressure equilibrium with their environment. (We find the alternative scenario in which all clouds have the same size but different densities less likely since the implied pressures would be very different and evaporation times could be embarrassingly short compared to the Hubble time; see the Appendix.) To this end we assume that the size of individual Mg II clouds is drawn from an intrinsic distribution $\phi(R_{\rm cloud})$ so that the observed distribution (taking into account cloud cross section effects on the detectability rates) is $\phi_{\rm obs}(R_{\rm cloud}) \propto \phi(R_{\rm cloud})R^2_{\rm cloud}$. A simple power-law distribution gives a reasonably good description of the data,

$$\phi(R_{\rm cloud}) \propto R^{\beta}_{\rm cloud}, \quad R^{\rm min}_{\rm cloud} < R_{\rm cloud} < R^{\rm max}_{\rm cloud}, \tag{7}$$

which implies a mass distribution,

$$\phi(M_{\rm cloud}) \propto M^{(\beta-2)/3}_{\rm cloud}, \quad M^{\rm min}_{\rm cloud} < M_{\rm cloud} < M^{\rm max}_{\rm cloud}, \tag{8}$$

where $M_{\rm cloud}$ is the mass of a single cloud. This distribution is defined for some minimum and maximum cloud size. We generate a population of clouds in the following way: in each rest equivalent width bin we randomly picked the sizes of $N_{\rm cloud}$ clouds drawn from ϕ and calculated their ionization structure and H I column densities. The total H I column of all clouds was then summed taking into account the scatter caused by intercepting a spherical cloud at various positions. This procedure resulted in one simulated point in Figure 4, which was then repeated over the entire rest equivalent width range spanned by the data. As we are only interested in modeling gas clouds in the halo of a galaxy, we did not model H I column densities $>10^{20}$ cm^{-2}, which likely arise in a galactic disk (Zwaan et al. 2005). We note that our estimates for the total mass of cool gas in the halos of galaxies will change by a factor of order unity by including the upper end of the column density distribution in our model. Given our density estimates from photoionization calculations and the constraints on the mean size of clouds, then a good fit for the Rao et al. (2006) data set is obtained for $R^{\rm min}_{\rm cloud} = 0.3$ kpc, $R^{\rm max}_{\rm cloud} = 1.5$ kpc, and $\beta = -2.5$ (corresponding to $\beta = -0.5$ for the observed distribution). Our approach allows us to reproduce the main observational trends summarized in Figure 4.

The gas temperature in our model is $\sim 10^4$ K and so the gas pressure is $P/k_{\rm B} \sim 200$ cm^{-3} K (similar to the value used by, e.g., Mo & Miralda-Escude [1996] and Gnat & Sternberg [2004] but somewhat lower than that implied by Fukugita & Peebles [2006]). The implied cloud mass distribution is $\phi(M_{\rm cloud}) \propto M^{-1.5}_{\rm cloud}$, with $M^{\rm min}_{\rm cloud} = 6 \times 10^4\, M_\odot$ and $M^{\rm max}_{\rm cloud} = 7 \times 10^6\, M_\odot$. Clouds are Jeans stable provided that the total mass (dark and baryonic matter) is $<10^8\, M_\odot$. The clouds are also relatively stable with respect to hydrodynamic instabilities (such as Klevin-Helmholtz) and evaporation (Maller & Bullock 2004).

In a typical Mg II–absorbing cloud, hydrogen is mostly ionized. Most of the metals are in singly or doubly ionized configurations. Nevertheless, the large total gas columns result in higher ionization levels having a nonnegligible column density. Specifically, the column density of C IV in our model can exceed 10^{13} cm^{-2}, which translates to an optical depth of order unity and is therefore consistent with a picture in which C IV absorption and Mg II absorption have a common origin. The uniform density clouds considered here cannot account for the strong intervening O VI $\lambda\lambda$1032, 1037 systems (see Danforth & Shull 2005; Bergeron & Herbert-Fort 2005), and an additional component/physics is required to explain them (e.g., Mo & Miralda-Escude 1996; McKee & Begelman 1990 and references therein).

In our analysis we have assumed that all clouds are exposed to a similar flux level regardless of their location in the halo. Nevertheless, the effect of shielding the ionizing flux by other clouds could be, in principal, important. A cloud located 50 kpc from a galaxy would see an effective column density of a few times 10^{18} cm^{-2} (corresponding to a few clouds). When shielding is included, as well as the contribution from the central galaxy, we find an overall decrease in the photoionization rate by a factor of $\sim$2 compared to the nonshielded case.

2.4. *Summary and Limitations of the Model*

As stated above, our model aims to provide a framework for studying the effects of a quasar radiation field on the absorption and emission properties of gas clouds in a galactic halo. The model has been calibrated using observational constraints on the spatial distribution of Mg II clouds within the halo of $\sim L^\star$ galaxies and the corresponding H I column densities. Our photoionization calculations have shown that the implied cloud parameters are consistent with the existence of Mg II–absorbing gas. We summarize the model parameters in Table 1.

This model leads to a picture in which $L^\star$ halos are filled with gas clouds that are partially ionized and sufficiently optically thick to be detected in both low- and high-ionization (e.g., C IV) absorption lines. These clouds have sizes of order 1 kpc, masses of $\sim 10^6\, M_\odot$, and particle densities of $\sim 10^{-2}$ cm^{-3}, amounting to a cool gas mass of $\sim 10^{11}\, M_\odot$ *within the virial radius*, i.e., $\sim$280 kpc at $z = 0$.

The results presented above assume that cool gas clouds are distributed throughout the entire volume of the halo up to the virial radius. Nevertheless, the virial radius has no clear physical connection to the scale, $r_{\rm cool}$, up to which cool clouds exist. In particular, the value of $r_{\rm cool}$ is expected to depend on the (unknown)

TABLE 1
Model Summary

Parameter	Value
Cloud Parameters	
Gas mass	$6\times10^4\ M_\odot < M_{\rm cloud} < 7\times10^6\ M_\odot$
Radius	0.3 kpc $< R_{\rm cloud} <$ 1.5 kpc
Density	$\rho_{\rm cloud} = 0.02$ atoms cm^{-3}
Metallicity	0.1 $Z_\odot$
Halo Parameters (20 kpc $< r < r_v$)	
Cool gas density profile	$\rho \propto r^{-2}$
Dark matter velocity dispersion	$\sigma = 140$ km s^{-1}
Virial radius[a]	$r_v = 282$ kpc
Virial mass	$M \simeq 10^{12}\ M_\odot$
Cool gas mass[b]	$M_{\rm cool} \lesssim 10^{11}\ M_\odot$
Number of clouds[b]	$\sim 7\times10^4$

[a] At $z = 0$.
[b] For a covering factor of unity and within r_v (see § 2.4).

origin of the cool gas. For example, if the gas is ejected from a galaxy, $r_{\rm cool}$ is likely to be smaller than if the gas was accreted from the intergalactic medium. Moreover, different values may be obtained if the cool gas condenses out of the virialized halo gas (e.g., Mo & Miralda-Escude 1996). At present, little is known with confidence about the origin of the cool gas, and observations provide only very loose constraints. Hence, $r_{\rm cool}$ is ill determined. Nevertheless, we find that the mass of cool gas in galaxy halos depends relatively weakly on $r_{\rm cool}$ for the relevant scale range. Specifically, to reproduce the covering factor statistics on large scales, we obtain $M_{\rm cool} \sim 3\times10^{10}$ $(4\times10^{10})\ M_\odot$ for $r_{\rm cool} = 50$ (100) kpc. Clearly, the mass of cool gas in galaxy halos is considerable for all plausible values of $r_{\rm cool}$ and a covering factor of order unity. In what follows we therefore assume that the gas occupies the entire virial volume (i.e., $r_{\rm cool} = r_v$).

Given our model assumptions and calibration constraints, the overall mass of cool gas, M, scales with the mean cloud size, $\langle R_{\rm cloud}\rangle$, and is inversely proportional to the assumed gas density. Our model is relatively insensitive to the metallicity provided that the gas composition is >0.01 solar so that the Mg II lines remain optically thick (see Fig. 3).

The physical origin of metal absorber systems is unknown. As such, it is not clear whether the cool clouds are transient, bound to dark matter minihalos, or in pressure equilibrium with their surroundings. In the latter case, we note that both the magnitude of the ambient thermal pressure in galaxy halos and its radial dependence are not well constrained and models suffer from various uncertainties related to both dark matter distribution (e.g., Nagai & Kravtsov 2005) and gas physics (e.g., Borgani et al. 2002; Hansen & Sommer-Larsen 2006; Dekel & Birnboim 2007). Hence, the total predicted mass in cool gas may change by a factor of order unity depending on model assumptions (while requiring agreement with observations). Given these uncertainties, we find our approximation of constant density clouds reasonable.

The total mass of cool gas depends on the assumed covering factor for absorption, which is a quantity still debated in the literature. We have used a covering factor of unity for strong Mg II absorption within ~50 kpc, as suggested by Steidel et al. (1997). However, other studies claim lower values (~0.2, Bechtold & Ellingson 1992; ~0.5, Tripp & Bowen 2005). As the total mass of cool gas scales linearly with this quantity, we might be overestimating the mass if the actual covering factor is not unity.

So far we have concentrated on modeling the cool gas within the halo of an $L^\star$ galaxy with $M_{\rm vir} = 2.5\times10^{12}\ M_\odot$. Our model *may* also be scaled to different galaxy luminosities and masses. Indeed, analyses by Steidel et al. (1997) and Guillemin & Bergeron (1997) have indicated that the normalization of the Mg II rest equivalent width follows a relation

$$W_0(r, L) = W_0(r)\left(\frac{L}{L^\star}\right)^\gamma, \tag{9}$$

with $\gamma \simeq 0.1$–0.4. Such a scaling has been reported in the luminosity range $0.3L^\star$–$5L^\star$ and at redshifts $0.5 < z < 1$. It is unclear whether the scaling should be extrapolated beyond these limits. The above relation may be understood within the framework of our model as a dependence of the number of clouds, and hence mass of cool gas, on luminosity. Denoting the mass of cool gas in $L^\star$ galaxies by $M^\star_{\rm cool}$, then the mass of cool gas in halos of galaxies with luminosity L may be written as

$$M_{\rm cool}(L) = f_M(L) M^\star_{\rm cool}, \tag{10}$$

where f_M is a dimensionless scaling factor.

3. QUASAR HALOS

We now investigate the effects of a quasar radiation field on the gas distribution within a halo and discuss the observational signature in absorption and emission. Our main assumption is that quasar halos are analogous to those of nonactive galaxies. As indicated by recent studies (e.g., Jahnke et al. 2004), the hosts of bright quasars seem to correspond to a few times $L^\star$ galaxies. Furthermore, Serber et al. (2006) find that bright quasars reside in overdense regions of galaxies, implying that their dark matter halos are several times those typical of $L^\star$ galaxies. Motivated by these studies, we allow f_M to deviate from unity. We show below that many observational constraints may be accommodated by using $f_M \sim 5$–10 for the mass of cool gas in quasar halos.

3.1. *Thermal and Ionization Structure*

In what follows we compute the time-*independent* ionization and thermal structure of a cloud exposed to a constant quasar ionizing flux. In the Appendix we present time-*dependent* calculations and show that the steady state assumption suffices for the luminosity range and the relevant spectral features considered here.

In modeling the spectral energy distribution (SED) of the quasar we have used the continuum defined by Sazonov et al. (2004), which is shown in Figure 2. Ionizing sources other than the quasar can be neglected. We start by introducing the ionization parameter, U, which is the ratio of photon density to particle number density and is a measure of the ionization level for photoionized gas. For the chosen SED we obtain

$$U \simeq 0.6 L_{46}\left(\frac{n}{10^{-2}\ {\rm cm}^{-3}}\right)^{-1}\left(\frac{r}{50\ {\rm kpc}}\right)^{-2}, \tag{11}$$

where the quasar luminosity is $L = 10^{46} L_{46}$ ergs s^{-1}. The ionization structure of several commonly detected ions as a function of U is shown in Figure 5. By combining these results with the density estimates from our model (§ 2), we can compute the ionization level and temperature as a function of the radius from the center of the QSO. The results for the temperature profile are shown in Figure 6. As expected, the quasar has a substantial effect on the thermal state of the inner parts of the halo and can heat the

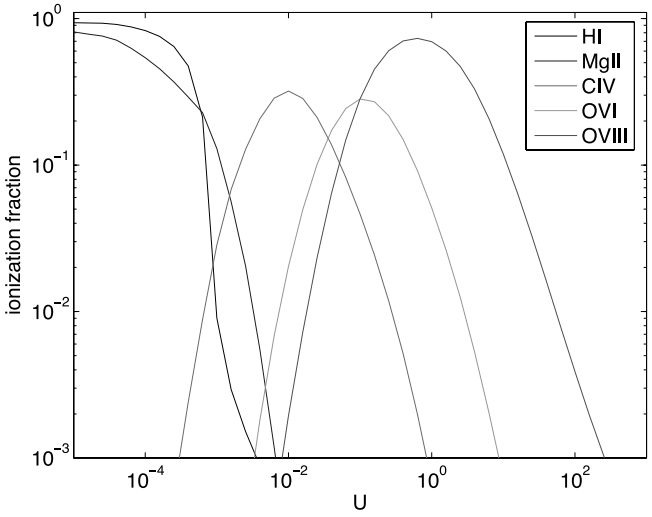

FIG. 5.—Ionization fraction of the abundant elements as a function of the ionization parameter, U. In this case the radiation field of the quasar overwhelms all other sources within ~10 Mpc of the quasar. Gas with the same density and distance as a typical Mg II–absorbing cloud would be highly ionized. [*See the electronic edition of the Journal for a color version of this figure*.]

(initially cool) gas to high temperatures by means of photoabsorption. The extent to which the Mg II halo is ionized depends mainly on the quasar luminosity. For example, a quasar with $L_{46} = 1$ heats gas within the inner 20 kpc to some 10^5 K, while gas at 50 kpc is ionized to a few times 10^4 K. Objects with Seyfert-like luminosities ($L_{46} \lesssim 0.1$) have a smaller effect on their immediate environments and heat the gas within their inner 20 kpc to a few times 10^4 K, while clouds at larger radii remain relatively cool. In contrast, very luminous quasars can heat clouds within 100 kpc to temperatures of order 10^5 K, with gas inside a radius of 10 kpc reaching the Compton temperature. The effect of a luminous quasar is not necessarily limited to halo gas, however, and low-density gas may be affected on much larger (megaparsec) scales. Our calculations indicate (Fig. 5) that for clouds to remain relatively cool within the central 30 kpc of an $L_{46} = 1$ source, their density should be $\gg 10^2$ cm^{-3}, i.e., considerably higher than the values considered here and those thought to be representative of Mg II clouds (cf. Stockton et al. 2002).

The ionization structure closely follows the temperature profile. Figure 6 shows the ionization fraction of several ions as a function of radius in the halo for the case of $L_{46} = 1$. Clearly, gas within the inner 100 kpc is devoid of Mg II ions, with C IV, O VI, and O VIII being most abundant; the ionization fraction of the latter peaks on the smallest scales. For an $f_M = 5$ halo with an $L_{46} = 1$ quasar (e.g., Jahnke et al. 2004; eq. [9]), the gas remains optically thin above the Lyman edge. For different source luminosities the abscissa of Figure 6 should be rescaled by L_{46}^{-1}. For low quasar luminosities ($L_{46} < 0.1$) even the inner regions of the halo remain at low temperatures and the gas is less affected by the quasar on ~100 kpc scales (see Fig. 6).

The active galactic nucleus (AGN) unification scheme (Antonucci 1993) suggests that quasars emit light in a double-cone geometry with an opening angle θ (see Fig. 7). Such an anisotropy in the radiation field will be imprinted in the properties of the gas distribution around the quasar. In the next sections we discuss the observational implications, in both absorption and emission.

3.2. *Quasar Halo Absorption Properties*

Clouds of gas that lie within the ionization cone of the quasar would be heated and ionized, and would follow the ionization structure presented in Figure 6. Therefore, the line of sight to a quasar would be largely devoid of Mg II absorption from the halo clouds modeled in this paper. Nevertheless, such highly ionized clouds are expected to give rise to associated absorption features from species like H I, C IV, and O VI, depending on their ionization structure, which is determined by the quasar luminosity, and their distance from the source. In contrast, lines of sight probing the quasar halo at finite impact parameters from the quasar would intercept cool gas that is not affected by the quasar radiation field and is therefore likely to show absorption features due to low-ionization

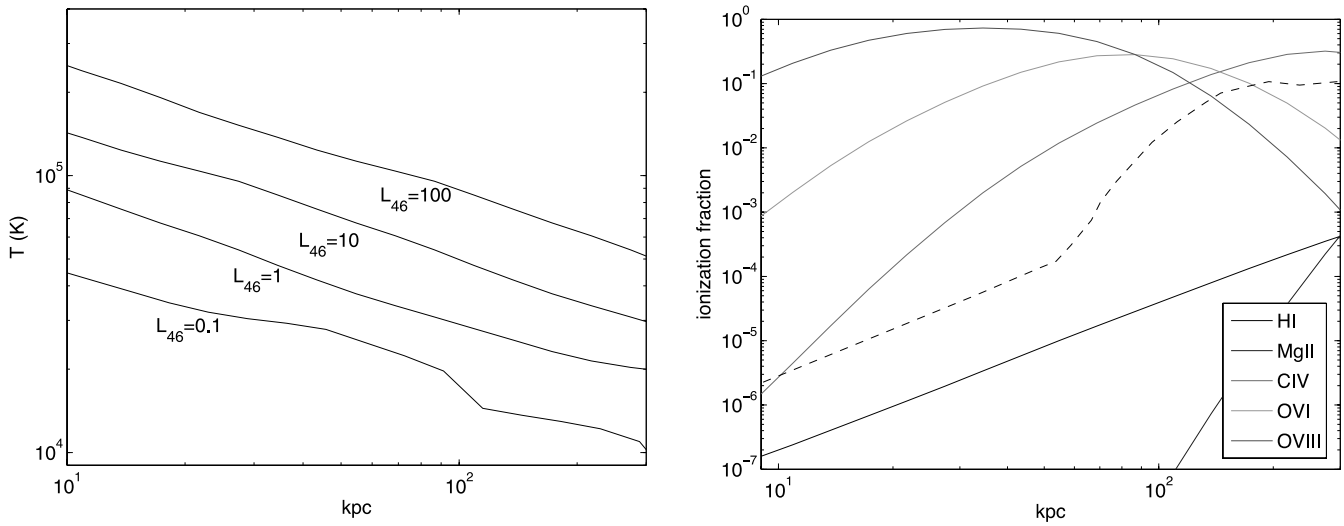

FIG. 6.—Thermal and ionization properties of halo gas ($f_M = 5$) illuminated by a quasar. *Left*: Temperature profile for a constant density, optically thin medium with density of 0.02 cm^{-3} (see text) for several values of quasar luminosity. Clearly, the temperature drops with distance as the ionization parameter decreases ($\propto r^{-2}$). The radiative effect of Seyfert galaxies on their environment is more localized than that of bright quasars. *Right*: Ionization structure as a function of distance from an $L_{46} = 1$ quasar. As expected, the ionization level decreases (i.e., the fraction of H I rises) with distance due to the dilution of the radiation field. The fraction of Mg II recovers only on megaparsec scales, while closer to the quasar (~100 kpc) C IV is expected to be seen; on smaller scales still (~20 kpc) O VI would be detected. The gas is very highly ionized within ~30 kpc and could be detected in X-rays. For quasars with different luminosities the abscissa should be rescaled by $L_{46}^{1/2}$. Thus, brighter quasars would ionize their environment to larger distances. The dashed line corresponds to the fraction of H I for the case of $L_{46} = 0.1$. The hump beyond ~50 kpc is the result of self-shielding (see text). [*See the electronic edition of the Journal for a color version of the right panel of this figure*.]

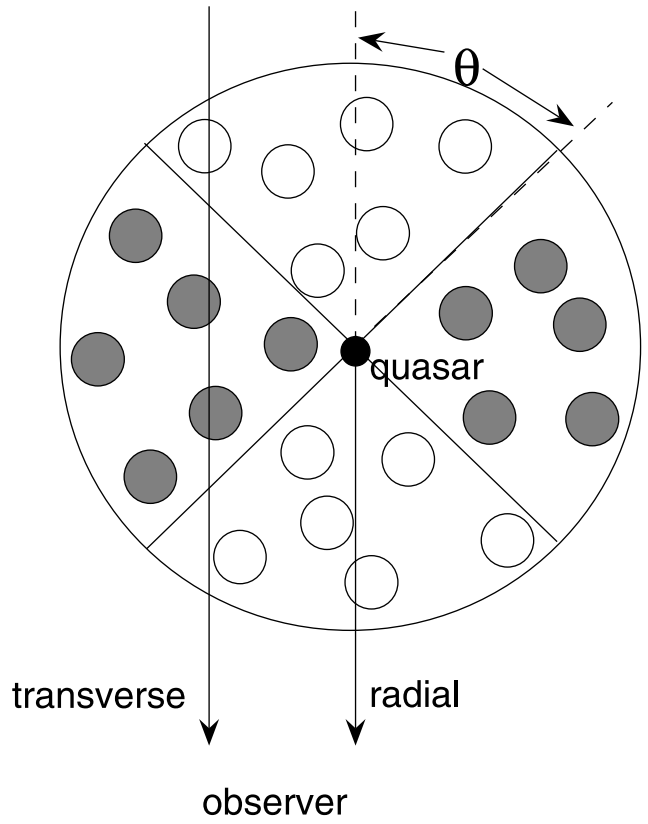

FIG. 7.— Cartoon showing the distribution of different types of gas clouds around a quasar, in relation to an observer's sight line. A quasar emits ionizing radiation into a cone with opening angle θ. Cool gas clouds that are exposed to the ionizing radiation are heated (*open circles*), while those that are shielded from the ionizing radiation remain cool (*filled circles*). The properties of the nonionized clouds resemble those of clouds in halos associated with nonactive galaxies. Off-center lines of sight will intercept cool gas in the transverse direction, while those that point radially toward the quasar will mostly see ionized gas (see text).

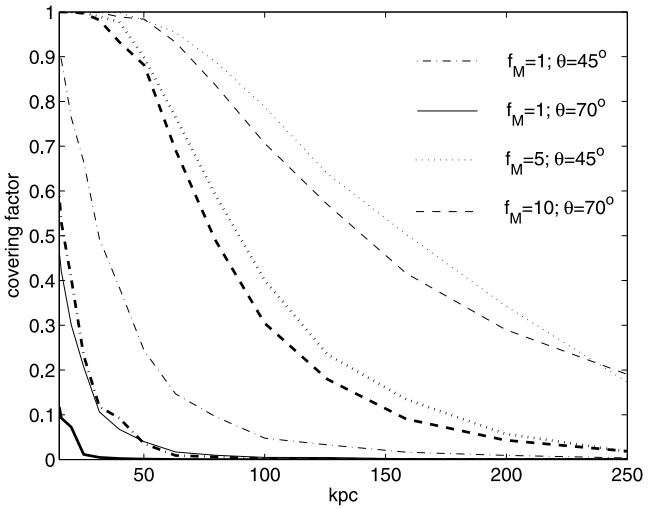

FIG. 8.—Covering factor for strong Mg II absorption as a function of the impact parameter for lines of sight passing through the halo of a quasar (see Fig. 7). Four halo models are considered that differ by the mass of cool gas within the virial radius (denoted by f_M; see text) and the opening angle, θ, of the quasar radiation field. For each model we calculate the covering factor for systems with $W_0 > 1$ Å (*thick lines*) and $W_0 > 0.6$ Å (*thin lines*). As expected, the covering factor declines with increasing impact parameter due to the decreasing cloud density with distance. The covering factor for strong absorption is sensitive to both θ and f_M. As θ increases, more gas is ionized and the halo becomes transparent to Mg II absorption. As f_M rises, more clouds are intercepted along lines of sight through the halo. As shown, different combinations of f_M and θ can result in a similar covering factor for strong Mg II absorption (see text).

species as those seen around nonactive galaxies. The number of Mg II clouds intercepted by a given sight line depends not only on the total number of clouds within the halo (which, for nonactive galaxies, depends on the galaxy luminosity; see eq. [9]) but also on the opening angle of the quasar.

Given the above model, we now discuss the observable properties of quasar halos in terms of their expected absorption signatures. In a recent work we used pairs of quasars at different redshifts to search for Mg II absorption in the spectrum of the background quasar at the redshift of the foreground quasar (Bowen et al. 2006). In four out of four cases we detected Mg II absorption at the correct redshift, with $W_0 > 0.5$ Å. This suggests that strong Mg II absorbers are common in the transverse direction of quasars. We have extended our analysis to a larger sample of systems, and our new results (Bowen et al. 2007) indicate the presence of strong Mg II absorption around quasars with a covering factor close to unity within 100 kpc, followed by a rapid decline at larger radii. Such behavior is similar to that of Mg II gas that is detected around galaxies. This high covering factor for Mg II gas in the transverse direction seems to be in contrast with smaller values ($\sim$10%) derived for Mg II absorption directly along quasar lines of sight (see Fig. 7). As we show below, this finding is naturally explained by our model.

Quasar radiation is thought to be emitted into cones of opening angle θ (Antonucci 1993). As such, θ is a measure of the mass of cool gas within the halo that is exposed to the ionizing field and determines the mass of the remaining cool gas. The connection between θ and W_0 is therefore apparent within the framework of the model (see Fig. 7). Model predictions for the absorption covering factor as a function of the rest equivalent width, the impact parameter, and the mass of cool gas, f_M, are given in Figure 8. These results are analogous to those of galaxies but for the additional dependence on θ. Quasars that emit more isotropically have less cool gas at any impact parameter due to ionization effects. More massive envelopes of cool gas have a larger number of clouds and so produce broader Mg II troughs. Clearly, different combinations of f_M and θ can yield similar covering fractions. At present, neither the mass of cool gas in quasar halos nor the opening angle of quasar ionization cones is well determined; recent surveys indicate that θ may depend on the quasar luminosity, with θ in the range $45^\circ < \theta < 70^\circ$ for bright quasars (Willott et al. 2000; Treister & Urry 2005). Figure 8 shows that $f_M \simeq 5$–10 is required to explain the high occurrence of transverse strong Mg II absorption around quasars within 100 kpc in the Bowen et al. (2006, 2007) sample.

We can further compare the predictions of our model to observations by considering the fraction of quasars showing associated absorption, i.e., absorption arising along the quasar line of sight close to the quasar redshift (Fig. 7). As mentioned above, in such a case, low-ionization species are not expected to be abundant due to rapid ionizations by the quasar radiation field. However, the same clouds are expected to give rise to higher ionization absorption lines. Figure 9 shows our predictions for the covering factor of H I, Mg II, C IV, and O VI lines as a function of (nonvirialized) gaseous halo mass and quasar luminosity. The covering factor for all lines is seen to decrease exponentially with increasing W_0 due to Poisson statistics. As shown, the covering factor for absorption is more sensitive to the quasar luminosity than to the mass of cool gas in the halo. In particular, the halos of more luminous quasars are more ionized, resulting in a lower covering factor for strong low-ionization systems. As expected, more massive gaseous halos produce stronger absorption lines due to the larger

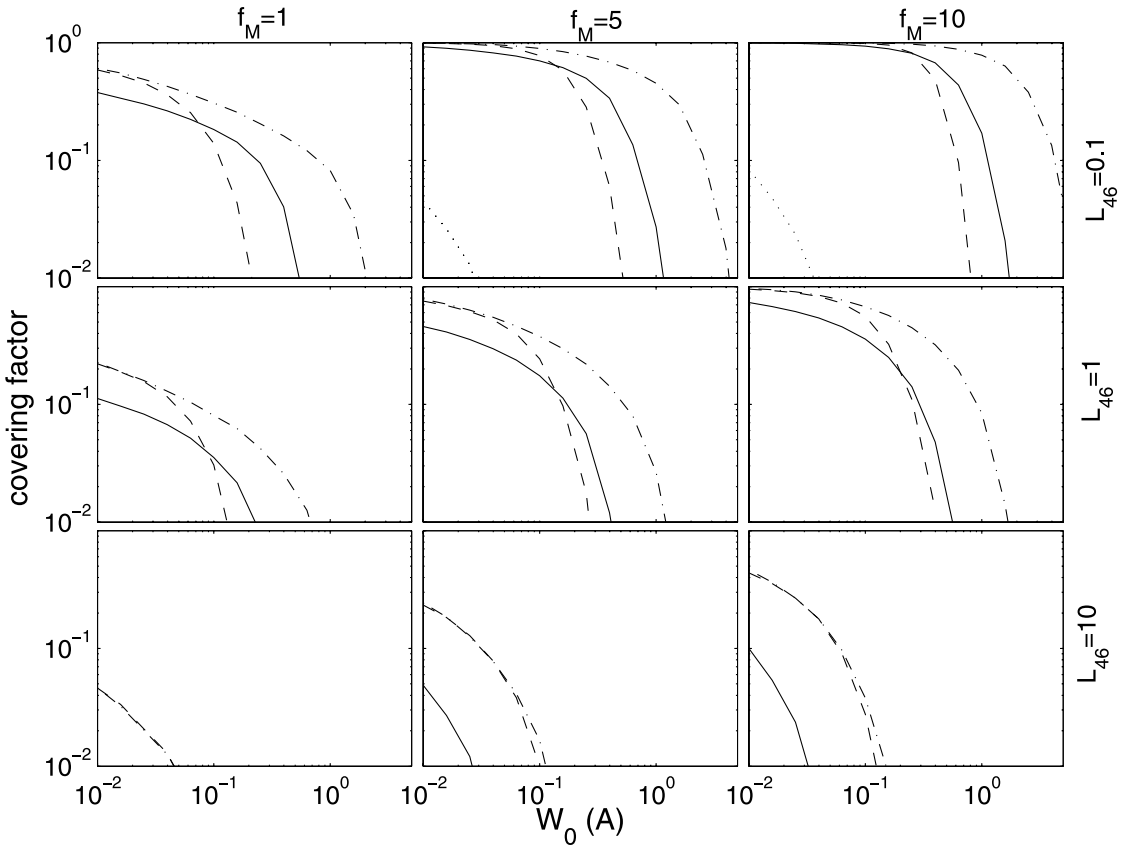

FIG. 9.— Predicted covering factor for associated absorption where lines of sight probe the ionized part of the halo. Covering factors for several high-ionization lines are considered, corresponding to H I Lyα (*dot-dashed line*), Mg II λ2796 (*dotted line*), C IV λ1548 (*solid line*), and O VI λ1032 (*dashed line*). The results are shown as a function of the quasar luminosity for $L_{46} = 0.1-10$ (*columns*) and mass in cool gas with $f_M = 1-10$. As shown, the covering factor is more sensitive to the luminosity than to the mass in cool gas. The covering factor follows the exponential cutoff of the Poisson distribution for the respective lines. Low-luminosity quasars have a higher covering factor for low-ionization lines since the halo is less ionized. For bright objects the halo is more ionized and low-ionization lines become weaker.

number of clouds intercepted along the line of sight. Our predictions appear to be in qualitative agreement with recent surveys indicating a covering factor of $\sim$30% for strong C IV absorption (Vestergaard 2003). Our model predicts little associated Mg II absorption due to halo gas. Our model does not, however, include the possibly important contribution from absorption by gas in the immediate vicinity of the black hole (sometimes termed "intrinsic" absorption). That said, our model is consistent with the notion that most low-ionization associated systems are intrinsic to the quasar. Additional data concerning the covering factor of various ionization stages as a function of quasar luminosity (and perhaps host mass) are required to test our model.

Radio galaxies provide a complementary configuration to the quasar pairs used by Bowen et al. (2006, 2007). For these objects our line of sight passes outside the quasar radiation cone. Measurements of large-scale H I absorption by Van Ojik et al. (1997) have shown that typical column densities through the neutral part of the halo are of order $\lesssim 10^{19}$ cm^{-2}. Such values are in qualitative agreement with our model and with the Rao et al. (2006) data set (see § 2). A more detailed comparison is unwarranted at this stage.

3.3. *Quasar Halo Emission Properties*

As the gas is photoexcited by the radiation field of the quasar, clouds would not only absorb but also emit and scatter continuum and line photons. In this section we calculate the expected emission-line flux from the halo.

Line emissivity depends on the ionization state of the gas, as well as on the optical depth through which line photons need to propagate, escape, and reach the observer. In calculating the emissivity of lines we have assumed that once line photons escape individual clouds, they reach the observer; i.e., we assume no photon scattering or absorption among different clouds. This approximation is adequate if clouds along our line of sight have little overlap in velocity space, which is the case considered in this paper. The fraction of line photons escaping from a single cloud was calculated using Cloudy using the escape probability method for a static cloud. The resulting emissivity per unit mass as a function of distance from the ionizing source is shown in Figure 10 for a Lyα emission line. As shown, averaged over volume, Lyα emissivity is relatively insensitive to the luminosity of the central object. This results from the gas temperature having only a weak dependence on luminosity for the relevant parameter range and from hydrogen being fully ionized. Emissivity is suppressed on small scales near very luminous sources due to suppression of the recombination rate at high ($\gg 10^5$ K) temperatures.

We have also studied the emissivity of other lines and, in particular, that of the [O III] λ5007 forbidden line (Fig. 10). The line emissivity in this case is very different from that of Lyα and other hydrogen-like lines since the recombination rate is much lower (O III and O IV abundances in the gas are negligible). Relatively neutral gas, which is required for efficient [O III] λ5007 emission, becomes abundant only on large scales and even then only for relatively low luminosity quasars. As quasars get brighter, the peak O III emissivity is shifted to larger scales where cooler gas is found. We emphasize that, unlike Lyα emission, [O III] λ5007 emission is sensitive to gas composition and is roughly linear with it.

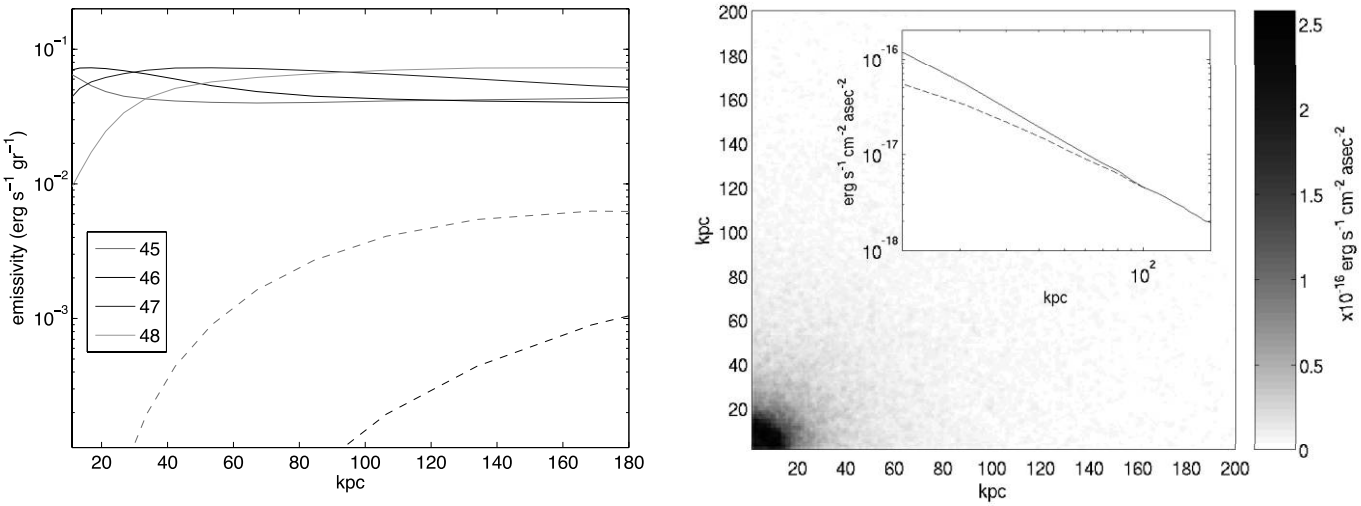

FIG. 10.—*Left*: Lyα (*solid lines*) and [O III] λ5007 (*dashed lines*) emissivities for various color-coded luminosities. While the Lyα emissivities of the nebulae at large radii are similar, the emissivity decreases with increasing quasar luminosity on smaller, $\lesssim$30 kpc scales due to ionization effects. The [O III] λ5007 emissivities are lower than those of Lyα and have their maxima at larger radii where cool gas is more abundant. *Right*: Lyα halo surrounding an $L_{46} = 1$ ($f_M = 5, \theta = 70^\circ$) quasar at $z = 1$ with gray scale reflecting the flux level. Also shown in an inset is the surface brightness profile including (*solid line*) and excluding (*dashed line*) scattering of Lyα photons from the broad emission line region of the quasar (see text). [*See the electronic edition of the Journal for a color version of the left panel of this figure.*]

Our calculations allow us to predict how quasar halos would appear for different emission lines. We show an example for a Lyα image in Figure 10 for the case of $\theta = 70^\circ, f_M = 5, L_{46} = 1$ and assume that our line of sight is along the symmetry axis of the quasar. The image is symmetric with the surface brightness profile being roughly $\propto b^{-1}$ from the center (neglecting the effects of scattering; see below). Asymmetric images are obtained if the axis of symmetry is at an angle to our line of sight, as likely to be the case in general.

Different lines have different emissivity profiles and hence different luminosities and inferred nebular sizes. Table 2 lists a few of the more important lines that could, in principal, be observed in quasar halos. Lyα, C IV λ1548, and O VI λ1035 are the strongest transitions, with the latter two lines depending roughly linearly on the metallicity. The typical nebular extent (from which most of the flux is emitted) of low-ionization lines is >100 kpc. This is in contrast to high-ionization line emission, which comes from compact, highly ionized regions of the halo (e.g., the nebular extent of O VIII X-ray lines is $\gtrsim$10 kpc for $L_{46} = 1$).

3.3.1. *Scattering of Quasar Photons in the Halo*

In addition to line emission, there is scattering (i.e., absorption followed by emission) of the photons emitted by the quasar. Here broad emission line photons can be scattered off gas clouds in the halo provided that the neutral hydrogen fraction is large enough. Owing to the low gas density, the population of excited levels is negligible and so only resonance lines are able to scatter efficiently. To correctly calculate the surface brightness profile due to photon scattering, one requires detailed knowledge of the three-dimensional distribution of clouds in real and velocity space. In addition, the fraction of photons reaching the halo depends on the amount of intrinsic absorption and the relative velocities of the emission line and halo gas. Detailed calculations should include the effect of multiple scatterings even in this relatively optically thin medium.

Despite the overall complexity of scattering problems, it is relatively straightforward to estimate the maximum scattered flux expected for different lines. This is simply the flux in the broad emission line with velocity dispersion, σ_l, that is intercepted by halo clouds with velocity dispersion, σ_c, given by roughly $\sigma_c/\sigma_l \simeq 10\%$ (here we used $\sigma_l \simeq 2000$; e.g., Vanden Berk et al. 2001). Given our quasar SED and taking the mean rest equivalent width for Lyα to be $\sim$90 Å (e.g., Zheng et al. 1997; Vanden Berk et al. 2001), we find that the maximum scattered Lyα luminosity is $L_{\mathrm{Ly}\alpha}^{\mathrm{scat,max}} \sim 2 \times 10^{43}(1 - \sin\theta)L_{46}$ ergs s^{-1}. Table 2 lists the results for other lines based on the same line of reasoning and shows that the contribution of scattered broad-line region photons to the large-scale nebular emission is probably less than 50% for all prominent lines (and for $L_{46} < 10^2$).

To better evaluate the flux due to broad emission line photons scattering off halo gas, we define an effective optical depth over the (dynamically broadened) absorption-line profile of halo gas, $\tau_{\mathrm{eff}}(r) = C(r)\tau(r)$, where $C(r)$ is the geometric covering factor of clouds at a given distance (i.e., the number of clouds intercepted at some distance interval) and $\tau(r)$ is the line optical depth of a single cloud at position r. In our model, $C(r)$ is large on small scales due to the cloud density peaking toward the center, yet $\tau(r)$ is low since the gas is more ionized. For Lyα, τ_{eff} is decreasing

TABLE 2
EMISSION-LINE PROPERTIES OF QUASAR NEBULAE

Line ID (1)	L (ergs s^{-1}) (2)	Size (kpc) (3)	$L^{\mathrm{scat,max}}/(L + L^{\mathrm{scat,max}})$ (4)
H I Lyα	3.0×10^{43}	150	0.25
O VI λ1035	4.4×10^{42}	80	0.25
N V λ1238	2.0×10^{42}	150	0.25
C IV λ1548	2.2×10^{42}	200	0.5
H I Hα	1.5×10^{42}	100	...
C III λ977	6.5×10^{41}	200	...
H I Hβ	5.3×10^{41}	100	...
O VIII λ18.97	3.5×10^{41}	20	?
[O III] λ5007	2.0×10^{41}	200	...

NOTES.—Col. (1): Emission-line identification. Col. (2): Luminosity of the emission line, with the luminosities for doublets taken to be the sum of individual transitions. Col. (3): Size of the emitting region, defined as the extent of the emitting nebula that contains 90% of the flux for a given transition. Col. (4): An order-of-magnitude estimate for the maximum luminosity in scattered light (see text). Transitions that do not scatter are marked with ellipses, while those for which the broad emission line flux is very uncertain are marked with a question mark (see text). $L_{46} = 1$, $\theta = 70^\circ$, and $f_M = 5$ are assumed.

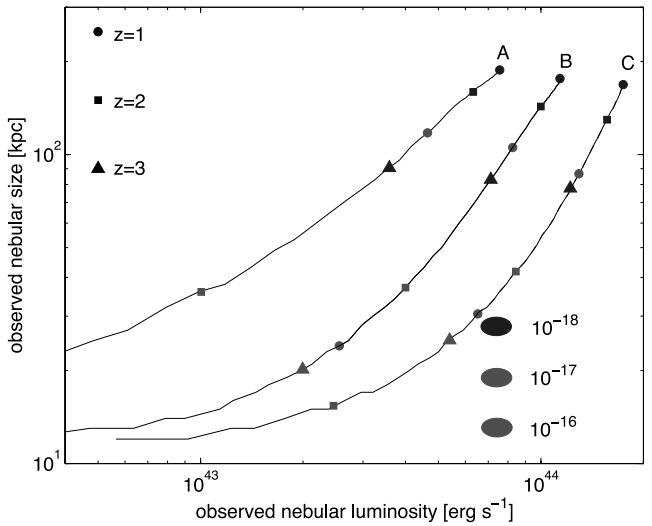

FIG. 11.—Observed Lyα nebula size (containing 90% of the total observed flux) vs. the observed luminosity for an $f_M = 10$ halo illuminated by an $L_{46} = 10$ quasar with an opening angle $\theta = 70^\circ$. The following models are considered: with no line scattering (model A); with scattered Lyα luminosity, $L^{\rm scat}_{{\rm Ly}\alpha} = 0.5L^{\rm scat,\,max}_{{\rm Ly}\alpha}$ (model B); and with $L^{\rm scat}_{{\rm Ly}\alpha} = L^{\rm scat,\,max}_{{\rm Ly}\alpha}$ (model C). We assume no evolution in the nebula properties with redshift. Placing the same nebula at different redshifts (denoted by different symbols; see legend) decreases its observed luminosity and size for a survey with a given limiting flux (denoted by gray scale in units of ergs s^{-1} cm^{-2} arcsec^{-2}). Clearly, unless the nebula is close and/or the sensitivity is high, only the brighter inner part of the nebula is observed, which results in an underestimation of its luminosity and size (see text). In particular, sensitivities of order 10^{-18} ergs s^{-1} cm^{-2} arcsec^{-2} are required to probe the full extent of quasar nebulae at $z \lesssim 2$ (*dark square and circle*). [*See the electronic edition of the Journal for a color version of this figure*.]

with decreasing r. On scales larger than $\sim$30 kpc, clouds become opaque to Lyα and $\tau_{\rm eff} \propto C \propto r^{-2}$. We have approximated the problem by running Monte Carlo simulations (e.g., Zheng & Miralda-Escudé 2002; Z. Zheng 2007, private communication) of photons emitted by a point source, being scattered off halo gas, and with $\tau_{\rm eff}$ of order a few and having the radial dependence described above. We find that the surface brightness of the scattered photons is $\propto b^{-2.5}$ and therefore that most of the scattering occurs in the inner nebular regions (within $\sim$30 kpc). The results are shown in the inset of Figure 10 for the case of $L_{46} = 1$. We note, however, that these provide only order-of-magnitude estimates since the gas kinematics in the central regions of the halo is uncertain.

3.3.2. *Detectability of Line-emitting Regions*

It is interesting to examine the detectability of line-emitting nebulae around quasars within the framework of our model. Here we focus on Lyα nebulosity and study its observed luminosity and size as a function of the limiting flux of the observation (see Fig. 11). As before, $f_M = 10$, $\theta = 70^\circ$, and $L_{46} = 10$ are assumed. We also examine the line emission at several redshifts assuming that the observed nebulae at those redshifts are similar, so that the surface brightness is $\propto (1+z)^4$. Our calculations indicate that the limiting flux required to observe extended Lyα emission around $z = 1$ quasars is $\sim 10^{-16}$ ergs s^{-1} cm^{-2} arcsec^{-2}. In particular, our model suggests that the observed nebular extent is sensitive to the limiting flux with a factor of 2 increase in sensitivity allowing us to detect emission from an order-of-magnitude larger volume. At low z, a limiting flux of a few times 10^{-18} ergs s^{-1} cm^{-2} arcsec^{-2} is required to probe the full extent of the nebulosity and correctly estimate its luminosity. Once the appropriate sensitivity is reached, our model suggests that large-scale emission-line nebulae in general, and Lyα nebulae in particular, should be a rather common phenomenon around quasars. More massive gaseous halos or quasars having wider ionization cones are better emitters and their halos can be observed to higher z. Our calculations suggest that Lyα scattering can have a substantial contribution to the observed luminosity (compare models A, B, and C in Fig. 11). Similar considerations also apply for metal lines whose detection can be used to put more stringent constraints on the ionization level of the emitting gas and estimate its mean metallicity. For example, the N v λ1238 emission line could have a flux comparable to that of Lyα for gas with metallicities greater than the solar value (see Table 2).

3.3.3. *Comparison with Observations*

Extended narrow-line emission around quasars and radio galaxies has been observed for more than two decades. Giant Lyα nebulae certainly exist around quasars out to radii of $\sim$100 kpc (Wampler et al. 1975; Stockton 1976; Bremer et al. 1992; Boroson et al. 1982, 1985; Bergeron et al. 1983; Stockton & MacKenty 1987; Reuland et al. 2003; Labiano et al. 2005). Early studies focused mostly on RLQs, but later ones found that radio-quiet quasars (RQQs) also show extended Lyα emission on large scales. For example, Hu et al. (1991) observed a sample of seven RQQs down to a limiting flux of 2×10^{-16} ergs s^{-1} cm^{-2} and found no extended Lyα emission. However, subsequent and more sensitive observations showed that the nebulae could indeed be found around RQQs (Weidinger et al. 2005; Bremer et al. 1992; Steidel et al. 1991; Hu et al. 1996; Petitjean et al. 1996) with Lyα luminosities in the range $(7-58) \times 10^{42}$ ergs s^{-1}, values that are largely consistent with our predictions in Figure 11. Christensen et al. (2006) reported Lyα luminosities from $z \sim 3$ nebulae that are of order $\sim 10^{43}$ ergs s^{-1} and extend out to a median radius of 15 kpc (with some nebulae extending out to 60 kpc) for a flux limit of $\sim 10^{-17}$ ergs cm^{-2} s^{-1} arcsec^{-2}. This is consistent with quasar halos having a considerable amount of gas in a cool form (model A in Fig. 11 corresponding to $f_M = 1$ with no line scattering is excluded by the data; cf. Binette et al. 2006). Christensen et al. (2006) placed limits on C IV line emission fluxes $\sim$10 times lower than Lyα. In our model this is roughly the predicted flux ratio of the lines for gas with 0.1 solar metallicity. Unfortunately, more detailed modeling is beyond the scope of this paper.

The statistical properties of quasar line emission nebulae and their underlying physics are poorly understood, and few models have been devised to account for them (e.g., Heckman et al. 1991a, 1991b). Common explanations for the existence of such nebulae include gas accretion onto the central object (Haiman & Rees 2001) and matter ejection by the quasar and its host galaxy (e.g., Heckman et al. 1991a, 1991b). Moreover, the interpretation of the data is controversial; while several teams have reported high pressures of order $P \sim 10^6$–10^7 cm^{-3} K for RLQs, a study by Fu & Stockton (2006) points to lower pressures, of order 10^4 cm^{-3} K. These estimates come from compact emission regions of [O II] and [O III] lines and from absorption by excited states (e.g., Hamann et al. 2001). In our model for the halo of an $L^\star$ galaxy the pressure is even lower, $P \sim$ few $\times 10^2$ cm^{-3}. It is possible that RLQs are different from RQQs given their overall higher Lyα luminosities (e.g., Christensen et al. 2006) and their apparently large X-ray and [O III] emission on small scales (e.g., Crawford & Fabian 1989). Our model predicts relatively faint and diffuse [O III] emission from the halo, which seems to be at odds with recent detections of [O II]– and [O III]–emitting filaments around RLQs (e.g., Fu & Stockton 2006 and references therein). Deep optical observations of low-z RQQs may help to determine whether there is a relatively dense

and filamentary structure in quasar halos in addition to the more diffuse component considered here.

4. DISCUSSION

4.1. *Galaxies*

Our model implies considerable mass in cool gas out to the virial radius of $L^\star$ galaxy halos at $z \sim 1$. As explained above, this assumes a unit covering factor for strong absorption within 50 kpc of the galaxy. The lower covering factors suggested by Bechtold & Ellingson (1992) and Tripp & Bowen (2005) would actually lead to an agreement between our model predictions and the results of Maller & Bullock (2004), who estimated the mass of cool gas in the Galaxy halo to be $2 \times 10^{10}\ M_\odot$ and argued for consistency with observations of high-velocity clouds (see also Putman 2006). At present, radio surveys do not possess the required sensitivity to probe low column density, diffuse H I gas in 21 cm emission at distances of $\sim$100 kpc from a galaxy. We caution, however, that it is not clear whether our model predictions for $z \sim 1$ objects are directly applicable to present-day galaxies. Nestor et al. (2005) find evidence for evolution of cool gas properties with cosmic time whereby the occurrence of strong systems appreciably declines from $z = 1$ to 0.5. Bowen et al. (1995) also showed that no Mg II can be found around nearby galaxies beyond $\sim$40 kpc. Understanding the distribution of cool gas around present-day galaxies will require extensive UV spectroscopic surveys of sight lines that probe a wide range of galaxy impact parameters.

The notion of massive galaxy halos has been promoted by Fukugita & Peebles (2006) to provide a solution to the missing baryon problem. In their model, the mass of hot gas is a few times $10^{11}\ M_\odot$ within the virial radius (see Fig. 12). A cool and condensed component exists in their model within the central 20 kpc whose mass is a few times $10^{10}\ M_\odot$. Their total (hot) gas mass estimates provide a natural explanation to the missing baryon problem and are consistent with a large range of observational constraints that are independent of those considered here. However, their model did not consider the possible existence of cool gas beyond the extent of the disk. The addition of the extended cool gas component introduced here fits in nicely within the Fukugita & Peebles (2006) picture and results in only a modest departure from it (see Fig. 12) in the sense that it is possible to reproduce a number of observational constraints from absorption-line studies, while not significantly changing the total amount of (hot) gas within the virial radius.

On scales much smaller than the virial radius, the cool gas mass predicted by our model is much lower since it scales linearly with radius (e.g., Fig. 12). Specifically, the mass within 30 kpc is $M_{\rm cool} < 10^{10}\ M_\odot$ and, by extrapolation to smaller scales, is comparable to that estimated by Martin (2006) for ultraluminous infrared galaxy outflows.

More work is needed to establish how much cool gas resides in the halos of present-day galaxies. Observationally, better estimates of the covering fraction of cool gas around galaxies are required, preferably as a function of galaxy type. On the theoretical side, numerical simulations of galaxy formation need to include realistic cooling rates and reach high resolutions to reliably trace cool and condensed forms of gas. Understanding the properties of the dilute, yet likely very massive, cool gas component in galaxy halos is essential for understanding galaxy formation and evolution.

4.2. *Quasars*

Quasars are known to reside in galaxies, yet their large-scale environments are poorly understood. The recent discovery of Mg II–absorbing gas around those objects (Bowen et al. 2006, 2007) suggests an interesting link between galaxy and quasar environments. This implies that the presence of a quasar can be used to shed light on the distribution of matter in the halos of galaxies.

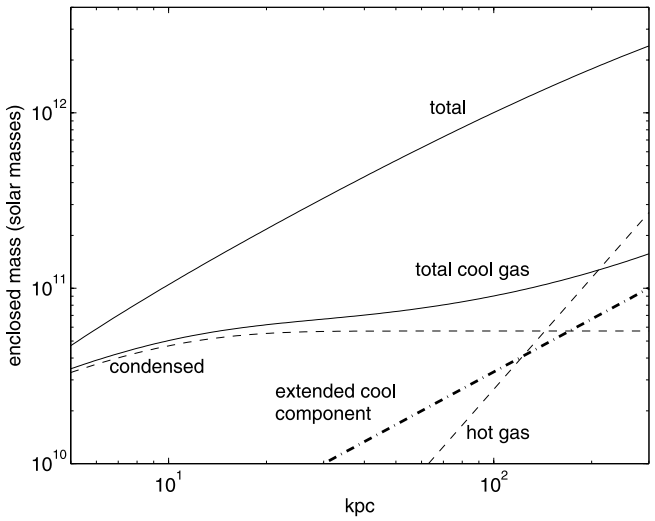

FIG. 12.—Extended cool gas component (*dot-dashed line*) considered in this work within the framework of the massive corona model by Fukugita & Peebles (2006; see their paper for the assumptions and physical motivation behind each of their components, shown as a dashed line). The total mass in cool gas is comparable to that of the hot component within the virial radius yet occupies only $\sim$1% of the volume. The total baryonic and dark matter mass for a typical $L^\star$ galaxy halo is also shown (see § 2.2 and Fukugita & Peebles 2006).

We have shown that it is possible to construct a model that unifies several distinct astrophysical phenomena pertaining to intervening absorption, associated absorption, and quasar emission nebulae. In our model, these phenomena are different manifestations of the same physical entity: cool gas condensations distributed within the halos of galaxies. If our model is correct, then the properties of cool gas in the vicinity of galaxies may be revealed by studying the influence of an active nucleus on its thermal and ionization structure. In particular, the study of associated absorption may help to constrain the density and distance of halo gas from the quasar. Cool gas around galaxies is notoriously difficult to detect in emission. Nevertheless, the presence of an ionizing source enhances emission and renders the detection of circumgalactic material more accessible. Furthermore, by studying the nebulosities around quasars, one can obtain a two-dimensional spatial by one-dimensional velocity picture of the gas. Mean quantities pertaining to the mass of the gas and its metallicity can be more easily deduced for individual objects.

In addition to shedding light on gas distribution in the halos of galaxies, it is possible to deduce important conclusions about quasar physics. For example, the recent results by Bowen et al. (2006, 2007) indicate a covering factor of order unity for cool gas in the transverse direction around quasars out to $\sim$100 kpc, in contrast to the much lower incidence of associated Mg II absorption along quasar sight lines. Our model implies that this is merely a consequence of the quasar unification scheme: gas in the radial direction to the quasar is heated to high temperatures, while that which is at right angles to the quasar ionization cone remains unaffected. This is not a trivial result since, although the unification scheme is well established for AGNs, it is less secure for bright quasars at high z. Further tests of this conjecture may be carried out by comparing model predictions to the occurrence of associated absorbers for a wide range of ionization levels, as well as by studying emission-line nebulae in detail.

Our model can reproduce the emission and absorption properties of quasar nebulae by requiring quasar gaseous halos to be

more extended and therefore more massive than those of $L^\star$ galaxies. (Note that we do not refer to the virialized gas component in those systems.) It is worth noting that Serber et al. (2006) find that the dark matter halos of bright quasars are a few times more massive than those of $L^\star$ galaxies. Finally, if the correlation found between the size of cool gaseous halos and galaxy luminosity (Steidel et al. 1997; Guillemin & Bergeron 1997) can be extended to quasars, then the size of quasar nebulae is consistent with their hosts being a few times $L^\star$ (Jahnke et al. 2004).

Better understanding quasar emission line nebulae may allow us to deduce the long-term light-curve behavior of quasars. This will require more complete knowledge of the matter distribution in quasar halos, which can be achieved through deep imaging and spatially resolved spectroscopy of quasar environments. The detection of orphan nebulae (where the active nucleus is obscured) may provide a new means for identifying type II quasars. Combining large samples of emitting and absorbing gaseous nebulae may allow us to statistically constrain the mass of cool gas in quasar halos, as well as the opening angle of the quasars themselves. This has implications for reionization and background radiation determination. A survey of emission-line nebulae around a large number of quasars may also reveal environmental differences among quasar types (e.g., the RQQ-RLQ dichotomy). The detection of metal emission lines may also permit estimates of the metallicity of gas in the halo and enable tests of models that predict the metal enrichment of galaxies and the intergalactic/intracluster medium.

5. SUMMARY

We have presented a phenomenological model for the distribution of cool gas around $L^\star$ galaxies, calibrated with a wide range of observational constraints from absorption-line studies (including the rest equivalent width distribution of Mg II absorption lines, H I column densities, etc.). We argue that the halos of $L^\star$ galaxies are filled with gaseous clouds of sizes $\sim$1 kpc, masses of $\sim 10^6\ M_\odot$, and particle densities of $\sim 10^{-2}$ cm^{-3}. The total amount of cool gas within the virial radius of an $L^\star$ galaxy depends on the covering factor for strong Mg II absorption (which is a matter of debate) and is likely to be in the range $10^{10}\ M_\odot < M_{\rm cool} < 10^{11}\ M_\odot$ within the virial radius.

By assuming self-similarity, we show that our model for the distribution of cool gas around galaxies, if appropriately scaled (by a factor of a few), can reproduce the properties of cool gas seen around quasars. Our model simultaneously provides an explanation for the Lyα nebulosities observed out to $\sim$100 kpc around quasars and the absorption-line properties of the cool gas. Comparison of model predictions with future surveys will shed light on the missing baryon problem and will deepen our understanding with respect to galaxy formation and quasar activation.

We thank Gary Ferland for creating and maintaining Cloudy as a publicly available code. We are grateful to Z. Zheng for invaluable help with the Lyα scattering calculations. We thank K. Jahnke, N. Murray, and D. York for commenting on an earlier version of this paper. We appreciate a thoughtful report by the referee. This research has been supported by NASA through a Chandra Postdoctoral Fellowship award PF4-50033. D. V. B. is funded through NASA Long Term Space Astrophysics grant NNG05GE26G.

APPENDIX

Here we describe the time-dependent ionization and thermal structure of an initially cool cloud that is exposed to a quasar's ionizing radiation. As the quasar phenomenon is short lived compared to the Hubble time (the quasar lifetime, $\tau_q \sim 10^7$ yr; e.g., Worseck & Wisotzki 2006), it is instructive to first consider a few relevant timescales of the problem:

1. The dynamical timescale of a halo of size $R_{\rm halo}$ at a virial temperature T_v (corresponding to some sound speed v_s) is

$$\tau_{\rm dyn} \sim \frac{R_{\rm halo}}{v_s} \simeq 10^9 \frac{r}{100\ {\rm kpc}} \left(\frac{T_v}{10^7\ {\rm K}}\right)^{-1/2}\ {\rm yr}. \tag{A1}$$

2. The sound crossing timescale for a cloud of size $2R_{\rm cloud}$ at temperature T is

$$\tau_{\rm cross} \sim \frac{2R_{\rm cloud}}{v_s} \simeq 10^8 \frac{R_{\rm cloud}}{1\ {\rm kpc}} \left(\frac{T}{10^4\ {\rm K}}\right)^{-1/2}\ {\rm yr}. \tag{A2}$$

3. The photoionization timescale for ion X is

$$\tau_{\rm ion}^X = \left[\int \frac{\sigma_X(E) L_E}{4\pi r^2 E}\, dE\right]^{-1} \sim 10^3 L_{46}^{-1} \left(\frac{r}{10^2\ {\rm kpc}}\right)^2\ {\rm yr}, \tag{A3}$$

where σ_X is the cross section, E is the energy, L_E is the flux per unit energy, and r is the distance from the quasar. We assumed a mean ionizing photon energy of $E = 10$ eV and an ionization cross section of 10^{-19} cm^2 (roughly that of Mg II).

4. The recombination timescale for ion X is

$$\tau_{\rm rec}^X = \frac{1}{n\alpha_X(T)} \sim 5 \times 10^4 \left(\frac{n}{0.02\ {\rm cm}^{-3}}\right)^{-1}\ {\rm yr}, \tag{A4}$$

where n is the number density of atoms and α_X is the recombination coefficient (taking only the radiative term for Mg II).

The photoionization and recombination timescales are the shortest in the problem. The cloud and halo dynamical timescales (approximated by the sound crossing time) are probably longer than the quasar lifetime, τ_q; hence, while the ionization structure of

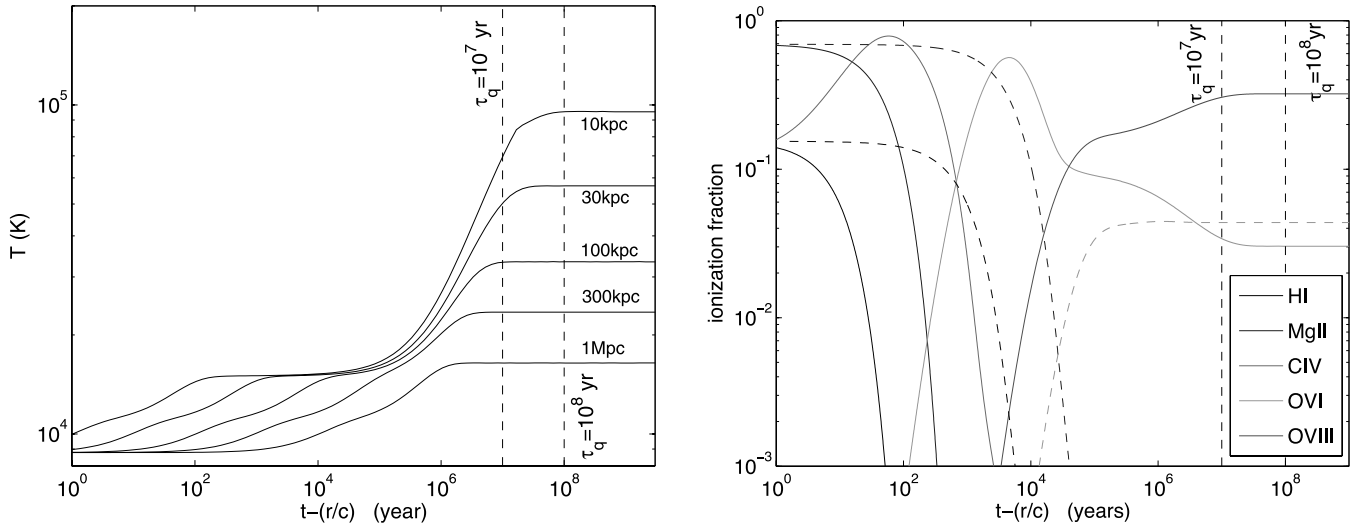

FIG. 13.—*Left*: Time-dependent thermal structure of the halo after a quasar ignites at $t = 0$ (and a cloud at a distance r from it is then exposed at time $t + r/c$) assuming $L_{46}(t) = \Theta(t)$, where $\Theta(t)$ is a step function. Also plotted are estimates for typical quasar lifetimes. Time-dependent photoionization effects are important and prevent the gas from reaching very high temperatures (close to the Compton temperature) over the quasar lifetime. *Right*: Ionization fractions for several abundant elements as a function of time. Gray scale denotes different ions (see legend), while different lines denote gas at different distances from the quasars: 30 kpc (*solid lines*) and 300 kpc (*dashed lines*). The rapid ionization of all low-level ions is clearly seen and takes place over $\lesssim 10^4$ yr. Such gas will therefore disappear from the line of sight and would become transparent. We note the general agreement between the ionization timescales obtained and the analytic approximation (eq. [A3]). [*See the electronic edition of the Journal for a color version of the right panel of this figure*.]

the clouds can vary rapidly (see below), the structure of the halo and embedded clouds remains approximately constant during the quasar lifetime. We note, however, that the sound crossing timescale for the smallest clouds in our model could be as short as $\sim 10^7$ yr if their temperature rises to high values once the quasar activates. We choose to ignore this complication here since (*a*) the quasar lifetime is poorly known and (*b*) the evaporation timescale is a few times the sound crossing timescale (e.g., Bertoldi 1989). Also, due to the spectrum of the cloud's size distribution, the evaporation of the smallest clouds will make little difference to our final conclusions.

In addition to the above analytic approximations, we have numerically computed several time-dependent photoionization and thermal models. This is necessary to quantify just how important the effects of the varying quasar flux are compared to time-independent calculations and to see which ions are affected most. The algorithm used for these calculations is fully described in Gnat & Sternberg (2007).

At the beginning of the calculation we assume that the cloud is exposed to the metagalactic field and is in ionization and thermal equilibrium. We then turn on a quasar and assume a step function description for its light curve, i.e., the quasar is off for $t < 0$ and on at $t \geq 0$. The quasar is assumed to maintain a constant flux level to $t \rightarrow \infty$. The calculations are carried out under isochoric conditions, as appropriate given the above considerations.

The thermal calculations are shown in Figure 13 for the case of $L_{46} = 1$ and demonstrate the limitations of the assumption of photoionization and thermal equilibrium. The gas heats up very quickly near the quasar where the ionizing flux is high and less so on larger scales. Typically, the gas within the inner 50 kpc heats up to $\sim 2 \times 10^4$ K over a period of $\sim 10^4$ yr (eqs. [A3] and [A4]). Further heating occurs on somewhat longer timescales that can be comparable to the quasar lifetime. Unless one happens to intercept young quasars, the inner 50 kpc region of the halo would be heated to $\lesssim 10^5$ K over the quasar lifetime. We conclude that, for moderate-luminosity quasars, the gas in the central regions of the halos can be efficiently heated to $\lesssim 10^5$ K. Nevertheless, further heating is delayed and may take longer than the quasar duty cycle or other relevant dynamical timescales of the problem. Assuming that τ_q is similar for all quasars, higher temperatures can be reached in the inner regions of the halos of bright quasars since the ionization timescale is shorter and the flux higher.

We have also calculated the time-dependent ionization structure of the halo and trace several of the ionization levels in Figure 13. As shown, all the low-ionization stages usually probed by absorption-line studies quickly attain negligible abundances and are not likely to be observed unless the quasar brightened over short timescales. For example, Mg II and H I would be immediately ionized and the gas is quickly heated. Time-dependent ionization deviations from a steady state solution can be important, but mainly for the high ionization levels, whose absorption lines would appear in the X-ray region of the quasar spectrum.

The above analysis suggests that it may be possible to treat the halos of quasars as having the same structure as galaxy halos since little structural changes are likely to occur over the quasar lifetime by radiation effects alone. We note that this may not be the case if quasar activity is a recurring phenomenon or if they have additional means of affecting their environment (via jets, winds, etc.). To conclude, for the purpose of this work, steady state photoionization calculations can be adequately used to describe the ionization and thermal state of the halo gas at all times.

REFERENCES

Antonucci, R. 1993, ARA&A, 31, 473
Badnell, N. R. 2006, A&A, 447, 389
Bahcall, J. N., & Spitzer, L. J. 1969, ApJ, 156, L63
Bechtold, J., & Ellingson, E. 1992, ApJ, 396, 20
Bergeron, J. 1986, A&A, 155, L8
Bergeron, J., & Boisse, P. 1991, A&A, 243, 344
Bergeron, J., Dennefeld, M., Boksenberg, A., & Tarenghi, M. 1983, MNRAS, 202, 125
Bergeron, J., & Herbert-Fort, S. 2005, in IAU Colloq. 199, Probing Galaxies through Quasar Absorption Lines, ed. P. R. Williams, C. Shu, & B. Ménard (Cambridge: Cambridge Univ. Press), 265
Bergeron, J., Kunth, D., & D'Odorico, S. 1987, A&A, 180, 1

Bergeron, J., & Stasinska, G. 1986, A&A, 169, 1
Bertoldi, F. 1989, ApJ, 346, 735
Binette, L., Wilman, R. J., Villar-Martín, M., Fosbury, R. A. E., Jarvis, M. J., & Röttgering, H. J. A. 2006, A&A, 459, 31
Bland-Hawthorn, J., & Maloney, P. R. 2001, ApJ, 550, L231
Borgani, S., Governato, F., Wadsley, J., Menci, N., Tozzi, P., Quinn, T., Stadel, J., & Lake, G. 2002, MNRAS, 336, 409
Boroson, T. A., Oke, J. B., & Green, R. F. 1982, ApJ, 263, 32
Boroson, T. A., Persson, S. E., & Oke, J. B. 1985, ApJ, 293, 120
Bowen, D. V., Blades, J. C., & Pettini, M. 1995, ApJ, 448, 634
Bowen, D. V., et al. 2006, ApJ, 645, L105
———. 2008, ApJ, submitted
Bremer, M. N., Fabian, A. C., Sargent, W. L. W., Steidel, C. C., Boksenberg, A., & Johnstone, R. M. 1992, MNRAS, 258, 23P
Bruzual, A., G., & Charlot, S. 1993, ApJ, 405, 538
Chabrier, G. 2003, PASP, 115, 763
Charlton, J. C., Mellon, R. R., Rigby, J. R., & Churchill, C. W. 2000, ApJ, 545, 635
Christensen, L., Jahnke, K., Wisotzki, L., & Sánchez, S. F. 2006, A&A, 459, 717
Churchill, C. W., Kacprzak, G. G., & Steidel, C. C. 2005, in IAU Colloq. 199, Probing Galaxies through Quasar Absorption Lines, ed. P. R. Williams, C. Shu, & B. Ménard (Cambridge: Cambridge Univ. Press), 24
Churchill, C. W., Mellon, R. R., Charlton, J. C., Jannuzi, B. T., Kirhakos, S., Steidel, C. C., & Schneider, D. P. 2000, ApJS, 130, 91
Churchill, C. W., & Vogt, S. S. 2001, AJ, 122, 679
Churchill, C. W., Vogt, S. S., & Charlton, J. C. 2003, AJ, 125, 98
Crawford, C. S., & Fabian, A. C. 1989, MNRAS, 239, 219
Crenshaw, D. M., Kraemer, S. B., & George, I. M. 2003, ARA&A, 41, 117
Cristiani, S. 1987, A&A, 175, L1
Danforth, C. W., & Shull, J. M. 2005, ApJ, 624, 555
Dekel, A., & Birnboim, Y. 2007, MNRAS, 383, 119
Diemand, J., Kuhlen, M., & Madau, P. 2007, ApJ, 667, 859
Ding, J., Charlton, J. C., Churchill, C. W., & Palma, C. 2003, ApJ, 590, 746
Ellison, S. L., Ibata, R., Pettini, M., Lewis, G. F., Aracil, B., Petitjean, P., & Srianand, R. 2004, A&A, 414, 79
Ferland, G. J., Korista, K. T., Verner, D. A., Ferguson, J. W., Kingdon, J. B., & Verner, E. M. 1998, PASP, 110, 761
Fu, H., & Stockton, A. 2006, ApJ, 650, 80
Fukugita, M., & Peebles, P. J. E. 2006, ApJ, 639, 590
Gehrels, N. 1986, ApJ, 303, 336
Gnat, O., & Sternberg, A. 2004, ApJ, 608, 229
———. 2007, ApJ, 168, 213
Guillemin, P., & Bergeron, J. 1997, A&A, 328, 499
Haardt, F., & Madau, P. 1996, ApJ, 461, 20
———. 2001, in 21st Moriond Astrophys. Meeting, Clusters of Galaxies and the High Redshift Universe Observed in X-Rays: Resent Results of *XMM-Newton* and *Chandra*, ed. D. M. Neumann & J. T. T. Van (Gif-sur-Yvette: Editions Frontières), 64
Haiman, Z., & Rees, M. J. 2001, ApJ, 556, 87
Hamann, F. W., Barlow, T. A., Chaffee, F. C., Foltz, C. B., & Weymann, R. J. 2001, ApJ, 550, 142
Hansen, S. H., & Sommer-Larsen, J. 2006, ApJ, 653, L17
Heckman, T. M., Lehnert, M. D., Miley, G. K., & van Breugel, W. 1991a, ApJ, 381, 373
Heckman, T. M., Miley, G. K., Lehnert, M. D., & van Breugel, W. 1991b, ApJ, 370, 78
Hu, E. M., McMahon, R. G., & Egami, E. 1996, ApJ, 459, L53
Hu, E. M., Songaila, A., Cowie, L. L., & Stockton, A. 1991, ApJ, 368, 28
Jahnke, K., Kuhlbrodt, B., & Wisotzki, L. 2004, MNRAS, 352, 399
Jahnke, K., & Wisotzki, L. 2003, MNRAS, 346, 304
Kacprzak, G. G., Churchill, C. W., Steidel, C. C., Murphy, M. T., & Evans, J. L. 2007, ApJ, 662, 909
Labiano, A., et al. 2005, A&A, 436, 493
Lanzetta, K. M., & Bowen, D. 1990, ApJ, 357, 321
Maller, A. H., & Bullock, J. S. 2004, MNRAS, 355, 694
Martin, C. L. 2006, ApJ, 647, 222
McKee, C. F., & Begelman, M. C. 1990, ApJ, 358, 392
Ménard, B., et al. 2008, MNRAS, 385, 1053
Mo, H. J., & Miralda-Escude, J. 1996, ApJ, 469, 589
Nagai, D., & Kravtsov, A. V. 2005, ApJ, 618, 557
Nestor, D. B., Turnshek, D. A., & Rao, S. M. 2005, ApJ, 628, 637
Norman, C., et al. 2004, ApJ, 607, 721
Oppenheimer, B. D., & Davé, R. 2006, MNRAS, 373, 1265
Petitjean, P., & Bergeron, J. 1990, A&A, 231, 309
———. 1994, A&A, 283, 759
Petitjean, P., Pécontal, E., Valls-Gabaud, D., & Chariot, S. 1996, Nature, 380, 411
Prochaska, J. X., & Wolfe, A. M. 1997, ApJ, 487, 73
———. 1998, ApJ, 507, 113
Prochter, G. E., Prochaska, J. X., & Burles, S. M. 2006, ApJ, 639, 766
Putman, M. E. 2006, ApJ, 645, 1164
Ranalli, P., Comastri, A., & Setti, G. 2003, A&A, 399, 39
Rao, S. M., Turnshek, D. A., & Nestor, D. B. 2006, ApJ, 636, 610
Rauch, M., Sargent, W. L. W., Barlow, T. A., & Simcoe, R. A. 2002, ApJ, 576, 45
Reuland, M., et al. 2003, ApJ, 592, 755
Sazonov, S. Y., Ostriker, J. P., & Sunyaev, R. A. 2004, MNRAS, 347, 144
Serber, W., Bahcall, N., Ménard, B., & Richards, G. 2006, ApJ, 643, 68
Steidel, C. C. 1993, in The Environment and Evolution of Galaxies, ed. J. M. Shull & H. A. Thronson (Dordrecht: Kluwer), 263
Steidel, C. C., Dickinson, M., Meyer, D. M., Adelberger, K. L., & Sembach, K. R. 1997, ApJ, 480, 568
Steidel, C. C., Dickinson, M., & Sargent, W. L. W. 1991, AJ, 101, 1187
Steidel, C. C., Kollmeier, J. A., Shapley, A. E., Churchill, C. W., Dickinson, M., & Pettini, M. 2002, ApJ, 570, 526
Steidel, C. C., & Sargent, W. L. W. 1992, ApJS, 80, 1
Sternberg, A., McKee, C. F., & Wolfire, M. G. 2002, ApJS, 143, 419
Stockton, A. 1976, ApJ, 205, L113
Stockton, A., & MacKenty, J. W. 1987, ApJ, 316, 584
Stockton, A., MacKenty, J. W., Hu, E. M., & Kim, T.-S. 2002, ApJ, 572, 735
Treister, E., & Urry, C. M. 2005, ApJ, 630, 115
Tripp, T. M., & Bowen, D. V. 2005, in IAU Colloq. 199, Probing Galaxies through Quasar Absorption Lines, ed. P. R. Williams, C. Shu, & B. Ménard (Cambridge: Cambridge Univ. Press), 5
Turnshek, D. A., Rao, S. M., Nestor, D. B., Belfort-Mihalyi, M., & Quider, A. M. 2005, in IAU Colloq. 199, Probing Galaxies through Quasar Absorption Lines, ed. P. R. Williams, C. Shu, & B. Ménard (Cambridge: Cambridge Univ. Press), 104
Vanden Berk, D. E., et al. 2001, AJ, 122, 549
van Ojik, R., Roettgering, H. J. A., Miley, G. K., & Hunstead, R. W. 1997, A&A, 317, 358
Vestergaard, M. 2003, ApJ, 599, 116
Wampler, E. J., Burbidge, E. M., Baldwin, J. A., & Robinson, L. B. 1975, ApJ, 198, L49
Weidinger, M., Møller, P., Fynbo, J. P. U., & Thomsen, B. 2005, A&A, 436, 825
Willott, C. J., Rawlings, S., Blundell, K. M., & Lacy, M. 2000, MNRAS, 316, 449
Worseck, G., & Wisotzki, L. 2006, A&A, 450, 495
York, D. G., Dopita, M., Green, R., & Bechtold, J. 1986, ApJ, 311, 610
York, D. G., et al. 2006, MNRAS, 367, 945
Zheng, W., Kriss, G. A., Telfer, R. C., Grimes, J. P., & Davidsen, A. F. 1997, ApJ, 475, 469
Zheng, Z., & Miralda-Escudé, J. 2002, ApJ, 578, 33
Zibetti, S., Ménard, B., Nestor, D., & Turnshek, D. 2005, ApJ, 631, L105
———. 2006, ApJ, in press
Zwaan, M. A., van der Hulst, J. M., Briggs, F. H., Verheijen, M. A. W., & Ryan-Weber, E. V. 2005, MNRAS, 364, 1467